Neoproterozoic High-K Calc-Alkaline Granitoids from Bapa-Batié, North Equatorial Fold Belt, Central Cameroon: Petrogenesis and Geodynamic Significance

Cyrille Chebeu[1], Christiane Diorlette Ngo Nlend[2], Jean Paul Nzenti[*,1] and Sylvestre Ganno[1]

[1]*Laboratory of Structural Geology and Petrology, Faculty of Science, University of Yaoundé I, P.O. Box 3412 Messa-Yaoundé, Cameroon*

[2]*Institute of Mineralogy and Geochemistry of Lausanne, University of Lausanne, Switzerland*

Abstract: Neoproterozoic granitoids of the Bapa-Batié area crop out within the Central Cameroon Shear Zone (CCSZ). They comprise four rocks: (i) granodiorite, (ii) biotite-granite, (iii) biotite-amphibole-granite, and (iv) granitic dyke. The elongated shape of the plutons and foliation striking parallel to the CCSZ point to syntectonic magma emplacement. The rocks are metaluminous, weakly peraluminous, high-K, and calc-alkaline to shoshonitic ferro-potassic, with mineralogical and geochemical characteristics of I-type granitoids. The rocks are characterized by high Ba, Sr, Zr, Rb, Sr, low Ni and Cr contents, and by variable LREE enrichment, moderate HREE fractionation with strong negative to moderate Eu anomalies (in granodiorite, biotite-granite and biotite-amphibole-granite) and moderate to significant positive Eu anomalies (in granitic enclaves). Trace element distribution patterns show that all these rocks are distinctively depleted in Nb, P, Sr and Ti relative to other trace elements and indicate that these rocks were derived from crustal protoliths. Magmatic zircon grains in these granites yielded LA-ICP-MS U-Pb ages of 600 ± 3.7 Ma and 619 ± 29 Ma. The plutonic rocks of Bapa-Batié area resemble other Neoproterozoic high-K calc-alkaline granites of Cameroon and also display strong similarities with high-K calc-alkaline plutons of eastern Nigeria and the Borborema Province in NE Brazil.

Keywords: Bapa-Batié neoproterozoic granitoids, central Cameroon shear zone, syntectonic magma emplacement, high-K and calc-alkaline magma, ferro-potassic series, I-type granitoids, LA-ICP-MS U-Pb ages.

INTRODUCTION

Granitoids display great diversity in their origin, sources and evolution processes and thus can be used as indicators of geodynamic environments and, in some cases as tracers of geodynamic evolution [1, 2]. The Pan-African North-Equatorial Fold Belt (PANEFB), or Central African Orogen, is a major Neoproterozoic Orogen linked to the Trans-Saharan Belt of western Africa and to the Brasiliano Orogen of northeastern Brazil (Fig. **1a**). In Cameroon, the Neoproterozoic realm [3-10] is subdivided into three domains from south to north (Fig. **1b**):

(1) The southern domain comprises Neoproterozoic metasedimentary units, such as the Ntui-Betamba, Yaoundé and Mbalmayo units; the protoliths of these units were deposited in a passive margin environment at the northern edge of the Congo Craton and were metamorphosed under high P conditions (T = 750-800°C, P = 0.9-1.3GPa) at 616 Ma [7, 11, 12]. Alkaline magmatism [13] has been also recognized in association with these Neoproterozoic units. The rocks of this southern domain were thrust onto the Archean Congo Craton towards the south [11, 14]. The thrust continues towards the east, forming the Oubanguides Nappe in the Republic of Central Africa.

(2) The central domain is positioned between the Sanaga Fault to the south and the Tibati-Banyo Fault to the north. These large NE-striking transcurent faults, as well as the Adamaoua Fault inside the central domain, are regarded as possible prolongations of the major shear zones of NE Brazil in a pre-drift Gondwana reconstruction [15-18]. This central domain consists of Paleoproterozoic high-grade gneisses (850-900°C, 1-1.2GPa) with Archean inheritance in the Palaeoproterozoic gneiss of Meiganga intruded by widespread Neoproterozoic syntectonic plutonic rocks of high-K calc-alkaline Affinities [4-6, 9, 19-24].

(3) The northern domain consists of subordinate 830 Ma-old metavolcanic rocks of tholeiitic and alkaline Affinities associated with metasedimentary rocks known as the Poli Series. Widespread 630-660 Ma calc-alkaline granitoids, now present as orthogneiss, result from a major episode of crustal accretion. A Palaeoproterozoic crustal source in this region is attested by the presence of 2 Ga inherited zircon domains in the granitoids [6, 25].

The study area around Bapa-Batié (~600 km^2, Fig. **2**) belongs to the southwestern part of the central domain. Conventional U-Pb zircon dating has yielded an age of 602 ± 1.4 Ma for this syntectonic Pan-African magmatism in the Batié area [26]. Some geochronological investigations have been carried out on some major magmatic complexes: the Ngondo granitic complex [19], Bandja charnockitic massif [18] and Bangwa granites [25] in the central domain; their emplacement ages vary from 557 ± 8 to 686 ± 17 Ma (Rb/Sr

*Address correspondence to this author at the Laboratory of Structural Geology and Petrology, Faculty of Science, University of Yaoundé I, P.O.Box 3412 Messa-Yaoundé, Cameroon; Tel: + 237 94 85 64 73; E-mails: jnzenti@uy1.uninet.cm, jnzenti2010@gmail.com

1874-2629/11

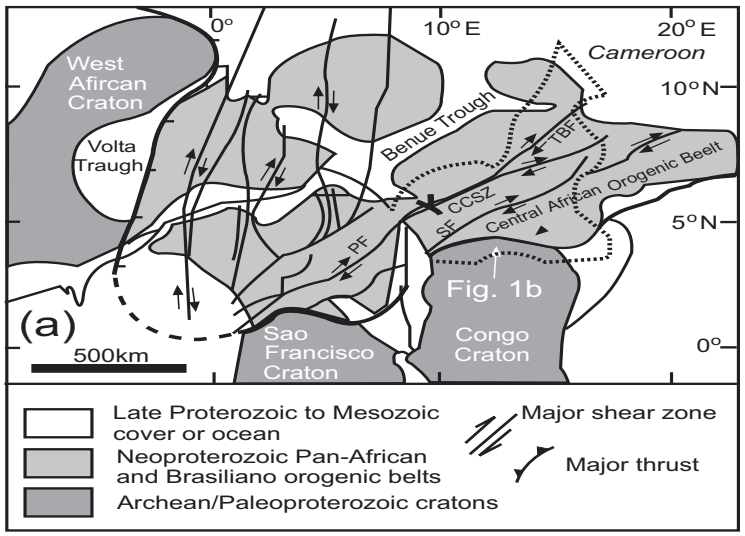

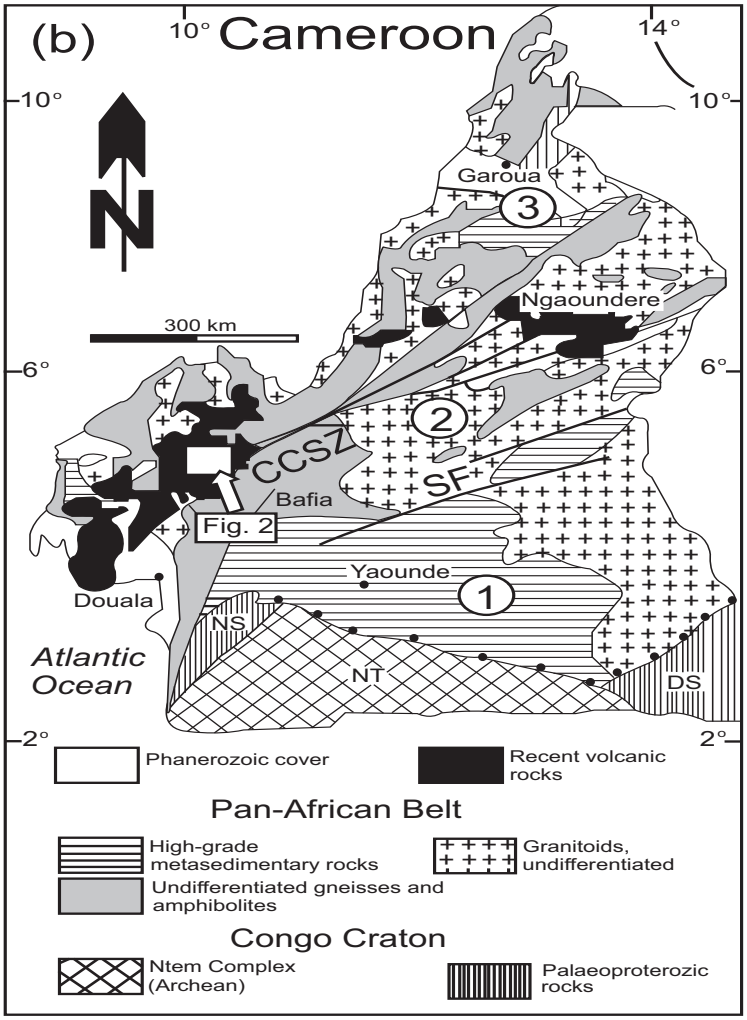

Fig. (1). (**a**) Geological reconstruction of Africa and NE Brazil (late-Precambrian) Afrter [68]. CCSZ: Cameroon Central Shear Zone; Pa: Patos shear zone; Pe: Pernambuco shear zone; SF: Sanaga fault; TBF: Tibati-Banyo Fault. (**b**) Geological map of Cameroon with the three main domains of the Pan-African orogenic belt (modified from [4, 69] and adapted from [5, 7, 9]: (**1**) southern domain corresponding to the Yaoundé series thrusted on the Congo Craton, (**2**) central domain, (**3**) northern domain. Granitoids suites are not distinguished due to large scale. CCSZ: Central Cameroon Shear Zone; DS: Dja series; NS: Nyong series; NT: Ntem Complex; SF: Sanaga Fault; TBF: Tibati-Banyo Fault. Location of study is marked by a square.

whole rock); an U-Pb zircon ages of 640 ± 15Ma and 638 ±2 Ma were obtained on the Bandja charnockite and Bangwa granite respectively. All these ages span the early stage of the deformation (orthogneisses) to the late uplift stages (post-tectonic massifs) of the Pan-African fold belt in Cameroon [9, 11, 19, 26].

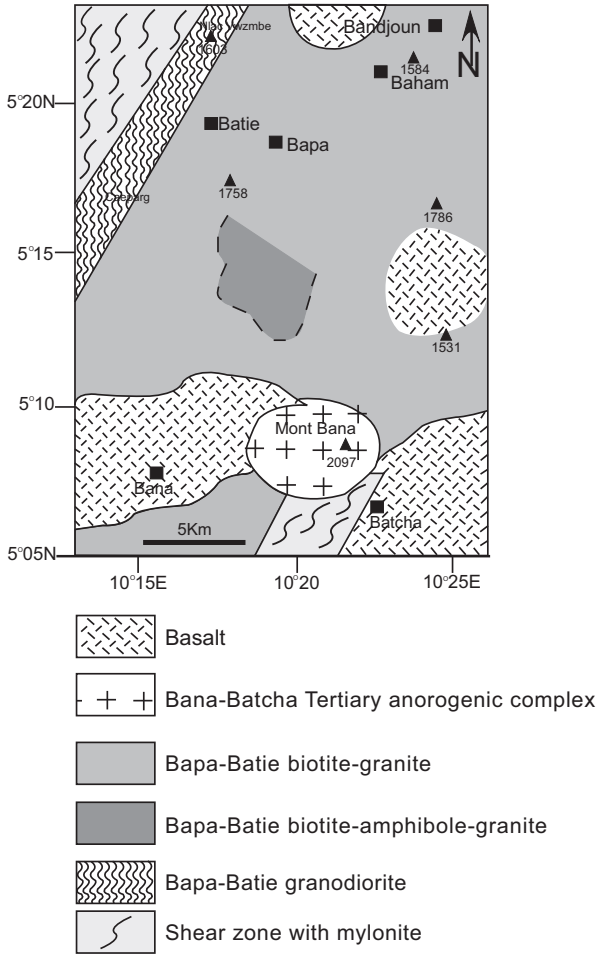

Fig. (2). Simplified geological map of the Bapa-Batié area.

In the present paper, geochemical, mineral chemistry and geochronological data of the plutonic rocks from the Bapa-Batié area in the southwestern part of the central domain of the PANEFB in Cameroon (Fig. **2**) are presented. The aim is to infer the specific geodynamic environment of the granitoids and their geodynamic significance in the PANEFB.

GEOLOGICAL SETTING

The Batié-Bapa complex (~600 km^2) is an NNE- to ENE-trending elliptically shaped massive that is partly deformed and consists of two units (Fig. **2**): 1) acidic rocks (biotite-granite, biotite-amphibole-granite) intruded by granitic veins; 2) intermediate rocks (gneissic granodiorite). The plutonic rocks intruded into layered gneiss during Neoproterozoic orogeny [27] at about 600 Ma [25]. The gneissic host rocks are metapelitic and metabasic units of Palaeoproterozoic age [3, 9, 23] that are grey or dark in color, and display alternating mm- to cm-scale quartzo-felsdpathic and garnet-kyanite-biotite- or garnet-sillimanite-biotite-rich layers. The host rocks were deformed during two main tectonic phases: the first phase (D_1) shows tangential tectonics with NW-SE kinematics direction, and is only recorded in the metamorphic rocks and absent in the granitoids. D_1 is marked by a flat mylonitic layering S_1 associated with an L_1 stretching lineation and F_1 isoclinals intrafolial folds. A mega-fold of regional scale reworked these structures. The second deformation event (D_2) was a tightening phase with NNE-SSW to ENE-WSW kinematics direction. The D_2 phase is recorded in both the metamorphic basement and granitoids. It is characterized by steeply dipping foliation planes roughly parallel to the general strike of the shear zone. The subhorizontal stretching mineral lineation and steep foliation planes are evidence for the dominantly transcurent nature of D_2. In the granitoids, the overall conformable nature of the foliation, either acquired during the magmatic stage or at the solid state, point to the syn-D_2 emplacement of the studied plutons. Although the strike values of the foliations are very similar, it is worth noting that their dips are less steep in the orthogneiss than in the shear zones proper. Recent work [8] shows that the study area in the central domain experienced transpressive tectonics during the Pan-African orogeny, resulting in a system of "décrochement-nappe" along the N70°E shear zone of the Adamaoua with an early sinistral sense of motion (D_2) that was later followed by a dextral sense of shear (D_3). While some workers [28, 29] in the eastern part of the Cameroon Central Domain have suggested that D_1 was a compressional event, D_2 also involved crustal compression and a peak metamorphic event. These deformation phases were overprinted by a late Pan-African transpression (D_3) event. The study area includes the shear zone (Fig. **2**): an N30°E shear zone passing through Chepang and Nkon Mwambe. It is important to discuss the spatio-temporal relationship of this ancient structure with these granitoids, the nature of the magmas, which produced it, and the significance of this shear zone in the geodynamic context of the Pan-African North Equatorial Fold Belt.

The Bapa-Batié massifs are made up of plutonic rocks, such as granodiorite (orthogneisses), biotite-granite (partly orthogneiss), biotite-amphibole granite and granitic dykes. Outcrops of the former country rocks are scarce, and intrusive contacts with the plutons are generally lacking.

ANALYTICAL METHODS

Microprobe analyses were carried out at the University of Lausanne with a CAMEBAX SX50. Counting times were 15-30 s per element on peak and 5-30 s on background depending on concentration. The accelerating voltage was 15 kV for a beam current of 10-20 nA, depending on the sample analyzed. The beam was rastered over a surface of 10 x 8 microns for feldspars and 3 x 2 microns for hydrated minerals. Natural silicates were used as standards.

Samples for whole-rock major and trace element analyses were crushed and subsequently reduced to a very fine powder by grinding in a tungsten carbide ring mill. Major and trace element concentrations of whole-rock from 34 samples were analyzed by X-ray fluorescence spectrometry

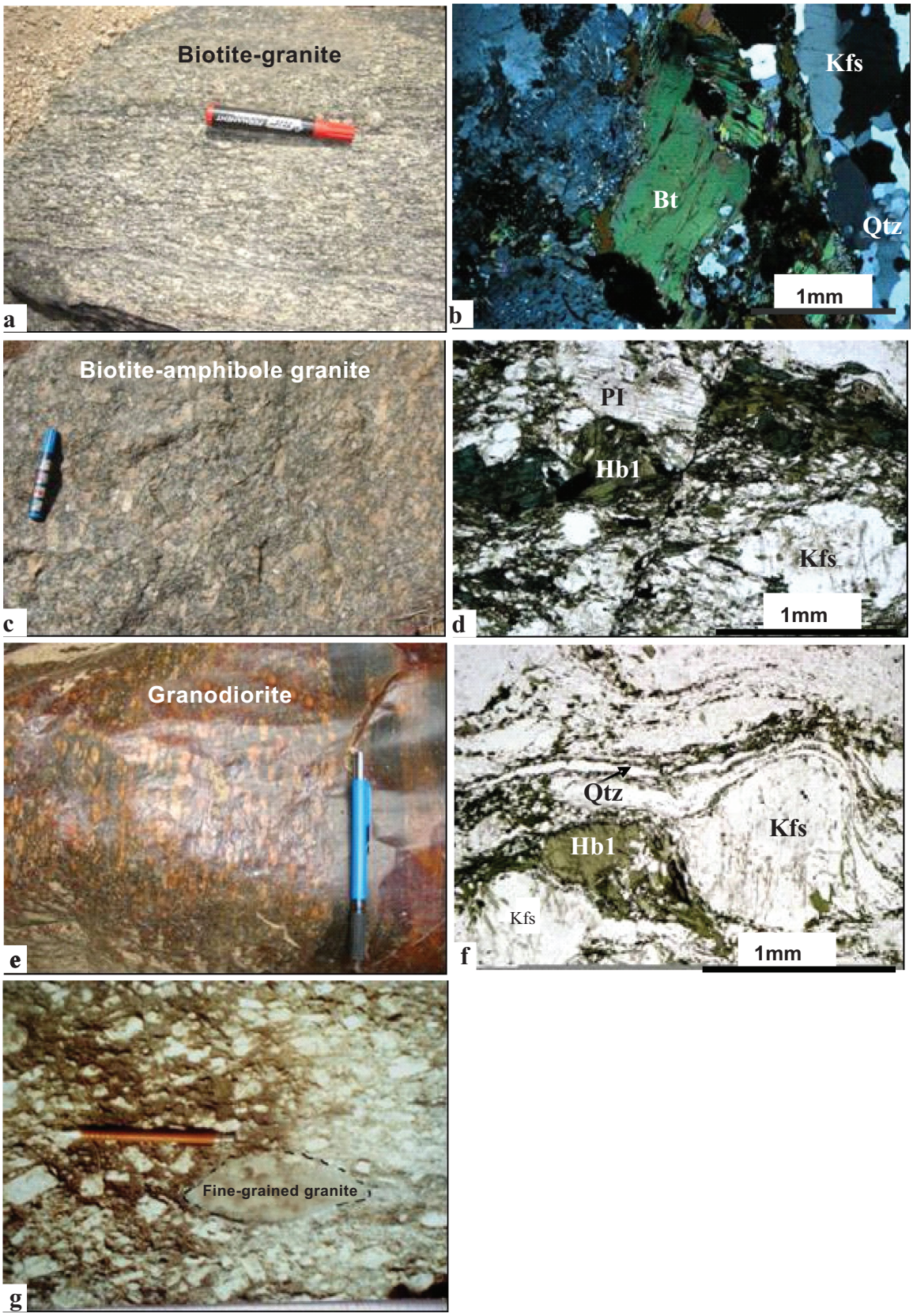

Fig. (3). Field occurrences and microscopic aspects of the granitoids in the Bapa-Batié area. (**a**) Aspect of Biotite-granite. (**b**) Detail of texture. (**c**) Biotite-amphibole- granite with grey pink color and megacrysts of Kfs. (**d**) Detail of mylonitic foliation with amphibole fish, feldspars porphyroblasts and recrystallisation of quartz. (**e**) Granodiorite showing strong mylonitic foliation. (**f**) Photomicrograph of gneissic granodiorite showing asymmetry K-feldspar with a sinistral shearing movement. (**g**) Fine-grained granite in enclave in biotite-granite. Bt = biotite; Kfs = orthoclase; pl = plagioclase; Hbl = hornblende; Qtz = quartz.

and LA-ICP-MS, at the University of Lausanne. Major elements (Si, Ti, Al, Fe, Mn, Mg, Ca, Na, K, P, Cr and Ni) were measured on fused lithium borate glass disks using a Philips PW2400 X-ray fluorescence spectrometer. Trace elements were measured from pressed powder pellets on the same XRF spectrometer (Nb, Zr, Y, Sr, U, Rb, Th, Pb, Ga, Ni, Cr, V, Ce, Ba and La), and by LA-ICP-MS on glass disks (Be, Sc, Ti, V, Cr, Ni, Cu, Zn, Y, Zr, Nb, Cs, La, Pr, Nd, Sm, Eu, Gd, Tb, Dy, Ho, Er, Tm, Yb, Lu, Hf, Ta, Pb, Th and U). Tests were made to assess the amount of trace element contamination, such as Ta and Nb, from the tungsten carbide mill. The samples analyses in this study are relatively rich in these elements, therefore contamination is considered negligible. Laser ablation measurements were made with a 193 nm Lambda Physik Excimer laser (Geolas 200M system) coupled to a Perkin-Elmer 6100 DRC ICP-MS. Laser settings were 27 kV with a 10 Hz repetition rate, yielding a fluorescence of about $12J/cm^2$ on the ablation site. Helium was used as carrier gas (1.1l/mn) and NIST612 glass was used as the external standard, and Ca and Al as internal standards (on the basis of electron microprobe measurements on the ablation pit site). BCR2 basaltic glass was regularly used as monitor to check for reproducibility and accuracy of the system. Results were always within ± 10% range of the values reported by Witt-Eickschen *et al*. (2003) [30], while Rb, Cs, Y and especially Cr were sometimes of the ± 10% range of the USGS recommended values for BCR2. Analytical uncertainties are currently better than 1% for major elements and 5-10% for trace element concentrations higher and lower than 20%, respectively. Analytical precision for rare earth elements (REE) is estimated at 5% when concentrations are >10 times chondritic and at 10% when lower.

LA-ICP-MS U-Pb Zircon Age

Zircon grains were separated using conventional techniques. After crushing and sieving of the powdered samples (250-90 μm fractions), heavy minerals were concentrated by panning and then by conventional heavy liquids and magnetic separation techniques. Non-magnetic crystals at 0 degree of lateral tilt on the isodynamic Frantz separator were examined under a binocular microscope and the most suitable grains were selected for analysis based on their high transparency, lack of mineral inclusions and cracks, euhedral shape and weakest coloration criteria. Zircon grains were heated at 850°C in the ambient atmosphere, and then treated with fluoridric acid (HF) and nitric acid (NHO_3) to remove surface impurities, mounted in epoxy resin and polished. Internal structure and morphology were subsequently observed by Scanning Electron Microscopy (SEM) and cathodoluminescence (CL) imaging using a CAMSCAN MV2300. Data were acquired at the Institute of Geochemistry and Mineralogy, University of Lausanne (Switzerland), using the LA-ICP-MS dating method with a 193mn Ar-F Geollas 200M excimer laser coupled to a Perkin Elmer Elan 6100 DRC. We employed both spot and profiling techniques depending on zircon grain size. Profile laser beam diameter varied between 25 μm for grains < 90 μm fraction and 35μm for grains 250-90 μm. Typical internal precision varied between 2 and 5% for the calculation of $^{207}Pb/^{235}U$ and $^{206}Pb/^{238}U$ ages, respectively, and was independent of the applied measurement mode. External well-characterized zircon reference standards (91500 and Plesovice) were monitored to measure routinely our grains during analytical session. The age obtained for the 91500 zircon standard is 1069.4 ± 5.9 MA (2σ, 23 analyses) that for the Plesovice standard is 337.8 ±1.9 MA (2σ, 34 analyses).

RESULTS

Petrography and Mineral Composition

Biotite-Granite

Biotite-granite (Fig. **3a**, **b**) is the most abundant rock type and consist of quartz (30-40 vol-%), plagioclase (10-15 vol-%), K-feldspar (20-30 vol-%), biotite (10-15 vol- %), accessory minerals (zircon, titanite, apatite) occur in very small proportions. Zircon is commonly present as inclusions in biotite and K-feldspar. Grain sizes are generally about a few millimeters, reaching as much as 2 cm; most samples are porphyritic with feldspar crystals up to 4 cm in length. Quartz occurs as polycrystalline ribbon with irregular grain boundaries or subgrain boundaries. Plagioclase (An_{17-27}, Table **1**) occurs as partly elongated, subhedral or rounded crystals. In some samples, plagioclase has inclusions of small euhedral biotite and zircon crystals. K-feldspar (Or_{90-95}, Table **2**) exhibit perthitic intergrowth; crystals are subhedral or rounded and oriented. K-feldspar has inclusions of small euhedral biotite, apatite and zircon crystals. Biotite (X_{Mg} = 0.39-0.54, Table **3**) occurs as flakes of various dimensions that may be clustered, most of which have corroded margins. Some crystals are kinked. Biotite has inclusions of small euhedral zircon and titanite crystals.

Biotite-Amphibole Granite

Biotite-amphibole-granite (Fig. **3c**, **d**) occurs as coarse-grained, grey-pink rock evenly grained with the following modal composition: quartz (35-45 vol-%), K-feldspar (20-25 vol-%), plagioclase (5-10 vol-%), biotite (5-10 vol-%), amphibole (10-20 vol-%) and titanite. Quartz is present as a large crystals or aggregates of quartz grains with undulose extinction. K-feldspar is orthoclase (Or_{91-92}, Table **2**), occurs as phenocrysts with as much as 4 cm length and exhibits, in places, perthitic exsolution. Plagioclase (An_{19-21}, Table **1**) forms sub- to anhedral grains (1.5 to 4 mm in length). Some grains show a bulbous symplectite of vermicular quartz (myrmekite). Plagioclase contains inclusions of apatite and zircon. Green hornblende (magnesiokatophorite, Table **4**) occurs as anhedral grains with development of minute grains of quartz and biotite at the grain boundaries. Amphibole contains numerous apatite and titanite inclusions. Biotite (X_{Mg} = 0.54-0.57, Table **3**) is present as lamellae replacing amphibole and contains small euhedral zircon inclusion. Titanite forms lozenge aggregates associated with amphibole and biotite.

Granodiorite

Gneissic granodiorite (Fig. **3e**, **f**) occupy the centre of the Chepang shear zone (elongate domain) in the northwestern area of the massif. In the field, granodiorite is usually a medium-grained, dark rock. It is characterized by pressure shadows on sides of K-feldspar megacrystals, strong planar-

Table 1. Representative Analyses of Plagioclase from Bapa-Batié Plutonic Rocks (wt%). Number of Ions on the Basis of 8 Oxygens

	Plagioclase							Granodiorite									Biotite- Granite				Biotite-Amphibole Granite			
N°	21	22	23	24	25	26	27	28	29	30	31	32	33	34	35	36	37	38	39	40	41	42	43	44
SiO_2	59.79	59.58	60.01	59.97	60.13	60.01	59.87	59.81	61.03	60.07	60.09	60.16	60.58	61.13	60.47	60.26	62.95	60.99	63.72	63.54	62.01	61.81	62.15	62.51
Al_2O_3	24.05	23.91	23.99	23.11	23.38	24.03	24.89	24.13	24.89	24.97	23.87	25.01	24.85	24.71	23.63	23.77	23.03	24.54	22.75	23.01	23.56	23.46	24.05	23.31
CaO	11.96	11.22	11.03	12.05	12.03	10.01	6.89	10.31	4.91	6.01	6.66	6.52	5.96	5.88	6.31	6.25	4.29	5.73	3.63	3.92	4.69	4.87	4.44	4.21
Na_2O	4.91	5.66	5.76	4.96	4.81	6.01	8.09	5.71	8.83	7.98	9.58	8.38	8.61	8.01	9.07	9.65	9.51	8.63	9.74	9.46	9.34	9.76	9.45	9.65
K_2O	0.16	0.18	0.11	0.13	0.21	0.23	0.55	0.21	0.35	0.53	0.11	0.13	0.21	0.25	0.17	0.15	0.09	0.19	0.13	0.11	0.21	0.24	0.19	0.31
Total	100.87	100.55	100.9	100.22	100.56	100.29	100.29	100.17	100.01	99.56	100.31	100.2	100.21	99.98	99.65	100.08	99.87	100.08	99.97	100.04	99.81	100.14	100.28	99.99
Si	2.6607	2.662	2.6686	2.6863	2.6832	2.679	2.671	2.6732	2.7108	2.6877	2.6875	2.6778	2.6931	2.7144	2.712	2.6979	2.7902	2.7108	2.8152	2.8053	2.7578	2.7442	2.5627	2.7712
Al	1.2613	1.2591	1.2573	1.22	1.2296	1.2643	1.3087	1.2711	1.303	1.3168	1.2582	1.312	1.302	1.2931	1.249	1.2542	1.2031	1.2855	1.1846	1.1973	1.2349	1.2276	1.1688	1.2179
Ca	0.5703	0.5371	0.5255	0.5783	0.5752	0.4788	0.3293	0.4937	0.2337	0.2881	0.3191	0.311	0.2839	0.2797	0.3032	0.2998	0.2037	0.2729	0.1718	0.1854	0.2235	0.2317	0.1962	0.2
K	0.0091	0.0103	0.0062	0.0074	0.012	0.0131	0.0313	0.012	0.0198	0.0303	0.0063	0.0074	0.0119	0.0142	0.0097	0.0086	0.0051	0.0108	0.0073	0.0062	0.0119	0.0136	0.01	0.0175
Na	0.4236	0.4903	0.4966	0.4308	0.4162	0.5202	0.6998	0.4948	0.7604	0.6923	0.8307	0.7232	0.7421	0.6896	0.7887	0.8377	0.8173	0.7437	0.8343	0.8098	0.8054	0.8401	0.7555	0.8294
X an	0.57	0.52	0.51	0.57	0.57	0.47	0.31	0.49	0.23	0.29	0.28	0.30	0.27	0.28	0.28	0.26	0.20	0.27	0.17	0.19	0.21	0.21	0.20	0.19
X ab	0.42	0.47	0.48	0.42	0.41	0.51	0.66	0.49	0.75	0.68	0.72	0.69	0.72	0.70	0.72	0.73	0.80	0.72	0.82	0.81	0.77	0.77	0.79	0.79
X or	0.01	0.01	0.01	0.01	0.01	0.01	0.03	0.01	0.02	0.03	0.01	0.01	0.01	0.01	0.01	0.01	0.00	0.01	0.01	0.01	0.01	0.01	0.01	0.02
	Labrador					Andesine		Oligoclase									Oligoclase				Oligoclase			

Table 2. Representative Analyses of K-Feldspar from Bapa-Batié Plutonic Rocks (wt%). Number of Ions on the Basis of 8 Oxygens

	Granodiorite							Biotite-Granite							Biotite-Amphibole Granite				
N°	1	2	3	4	5	6	7	8	10	11	12	13	14	15	16	17	18	19	20
SiO_2	65.04	65.13	65.23	64.98	64.91	65.11	64.98	63.89	64.74	64.91	64.04	65.03	64.65	64.85	64.91	65.03	65.01	64.04	64.45
Al_2O_3	19.02	18.86	18.87	18.95	19.03	19.03	18.86	18.72	18.65	18.48	18.74	18.65	18.96	18.86	18.55	18.43	18.64	18.87	18.94
CaO	0.02	0.03	0.01	0	0.01	0.03	0.01	0	0	0	0	0	0	0	0	0	0	0	0
Na_2O	0.71	1.01	0	0.81	0.75	0.79	1.01	0.56	1.12	0.56	0.58	0.56	0.51	0.76	0.86	0.91	0.91	1.02	0.98
K_2O	15.29	15.31	15.93	15.21	15.46	15.22	15.36	16.42	15.24	15.91	16.19	15.98	15.76	15.58	15.84	15.65	15.63	16.25	15.69
Total	100.08	100.34	100.04	99.95	100.16	100.2	100.22	99.59	99.75	99.86	99.55	100.22	99.88	100.05	100.16	100.02	100.19	100.18	100.06
Si	2.9875	2.9066	2.7925	2.9283	2.8199	2.9135	2.9014	2.9735	2.9893	2.9985	2.9769	2.9939	2.9833	2.9865	2.9921	2.9984	2.9920	2.9649	2.9745
Al	1.0296	1.1018	1.2338	1.0883	1.1965	1.1039	1.1067	1.0268	1.0149	1.0061	1.0267	1.0119	1.0311	1.0236	1.0078	1.0015	1.0111	1.0296	1.0302
Ca	0.0010	0.0016	0.0006	0.0000	0.0006	0.0016	0.0005	0.0000	0.0000	0.0000	0.0000	0.0000	0.0000	0.0000	0.0000	0.0000	0.0000	0.0000	0.0000
K	0.8960	0.9681	1.1274	0.9455	1.0522	0.9557	0.9756	0.9749	0.8977	0.9376	0.9601	0.9386	0.9278	0.9153	0.9315	0.9205	0.9177	0.9598	0.9238
Na	0.0632	0.0971	0.0000	0.0765	0.0776	0.0754	0.0975	0.0505	0.1003	0.0502	0.0523	0.0500	0.0456	0.0679	0.0769	0.0814	0.0812	0.0916	0.0877
X or	0.93	0.91	0.99	0.93	0.93	0.93	0.91	0.95	0.90	0.95	0.95	0.95	0.95	0.93	0.92	0.92	0.92	0.91	0.91
X an	0.00	0.00	0.00	0.00	0.00	0.00	0.00	0.00	0.00	0.00	0.00	0.00	0.00	0.00	0	0	0	0	0
X ab	0.07	0.09	0.01	0.07	0.07	0.07	0.09	0.05	0.10	0.05	0.05	0.05	0.05	0.07	0.08	0.08	0.08	0.09	0.09
	Orthoclase																		

preferred orientation of biotite and amphibole, and quartz grains flattened and/or elongate, and a common development of C-S structures. It is composed of quartz (15-25 vol-%), K-feldspar (10-15 vol-%), plagioclase (50-60 vol-%), biotite (15-20 vol-%), amphibole (5-10 vol-%); Accessory minerals include titanite and oxides (~ 2 vol-%). Quartz forms oriented single or platy crystals, polycrystalline ribbons or small rounded ones (0.1-0.3mm in diameter). K-feldspar (Or_{91-99}, Table **2**) occurs as elongate crystals (6 x 3mm to 0.4 x 0.2mm) or almond-shape with small flakes of biotite in inclusion. Bulbous symplectite of vermicular quartz (myrmekite) in K-feldspar is common. Tabular plagioclase (An_{23-49}, Table **1**) grains vary in size, reaching as much as 2mm, and have inclusions of small grains of quartz and biotite. Biotite (X_{Mg}= 0.47-0.54, Table **3**) forms platy flakes (2 x 0.8mm to 0.8 x 0.3mm) and has inclusions of euhedral titanite. Green hornblende grains (katophorite and magnesiokatophorite, Table **4**) are up to 1.5 mm in the length, show retrograde alteration to biotite and oxides, and

Table 3. Representative Analyses of Biotite from Bapa-Batié Plutonic Rocks (wt%). Number of Ions on the Basis of 22 Oxygens

	Biotite-Granite													Biotite-Amphibole Granite						
N°	20	21	22	23	24	25	26	27	28	29	30	31	32	33	34	35	36	37	38	39
SiO_2	36.45	36.07	35.99	35.69	35.74	36.27	35.46	36.77	36.11	36.39	36.67	36.17	36.41	36.01	36.05	36.05	36.51	36.63	35.98	36.01
TiO_2	1.75	2.44	2.46	2.93	2.38	2.66	2.81	2.54	2.66	2.91	2.87	2.71	2.83	1.38	1.51	1.56	1.63	1.65	2.21	2.23
Al_2O_3	16.31	15.96	16.63	16.44	16.36	15.93	15.98	16.11	16.03	16.13	16.21	15.98	16.01	15.11	15.05	15.21	15.11	15.45	15.33	15.44
FeO	21.01	22.94	22.99	22.4	23.56	23.02	23.07	23.01	23.58	22.85	22.51	24.27	24.09	19.13	19.22	19.21	19.43	19.35	19.85	19.82
MgO	11.13	9.68	9.52	9.55	9.51	8.44	8.96	9.01	9.34	9.51	9.66	8.69	9.01	14.26	14.19	13.67	14.11	13.99	13.98	14.35
MnO	0.21	0.31	0.34	0.28	0.21	0.29	0.26	0.34	0.31	0.34	0.28	0.29	0.31	0.35	0.31	0.35	0.28	0.25	0.31	0.36
K_2O	9.34	9.32	9.35	9.58	9.59	9.43	9.47	9.78	9.61	9.88	9.76	9.87	9.41	9.65	9.65	9.26	9.34	9.53	9.51	9.44
Total	96.2	96.72	97.28	96.87	97.35	96.04	96.01	97.56	97.64	98.01	97.96	97.98	98.07	95.89	95.98	95.31	96.41	96.85	97.17	97.65
Mg	0.4305	0.4541	0.3713	0.4541	0.3704	0.4541	0.3481	0.4541	0.3658	0.4541	0.3783	0.4541	0.3518	0.5374	0.4541	0.5194	0.4541	0.5229	0.4541	0.5294
Fe	0.4558	0.3897	0.503	0.3897	0.5148	0.3897	0.5464	0.3897	0.518	0.3897	0.4945	0.3897	0.5277	0.4044	0.3897	0.4094	0.3897	0.4057	0.3897	0.4102
Ti	0.0341	0.0287	0.0484	0.0287	0.0468	0.0287	0.0551	0.0287	0.0526	0.0287	0.0567	0.0287	0.0558	0.0262	0.0287	0.0299	0.0287	0.0311	0.0287	0.0415
AlVI	0.0796	0.1276	0.0773	0.1276	0.0679	0.1276	0.0505	0.1276	0.0636	0.1276	0.0705	0.1276	0.0647	0.032	0.1276	0.0413	0.1276	0.0403	0.1276	0.0189
K	1	0.9782	1	0.9782	1	0.9782	1	0.9782	1	0.9782	1	0.9782	1	1	0.9782	1	0.9782	1	0.9782	1
X_{Mg}	0.49	0.54	0.42	0.54	0.42	0.54	0.39	0.54	0.41	0.54	0.43	0.54	0.40	0.57	0.54	0.56	0.54	0.56	0.54	0.56

	Granodiorite																		
N°	1	2	3	4	5	6	7	8	9	10	11	12	13	14	15	16	17	18	19
SiO_2	36.71	35.97	36.81	36.51	36.61	36.17	36.36	36.54	36.35	36.41	36.56	36.51	36.71	36.78	36.65	36.08	36.53	36.21	36.41
TiO_2	1.89	1.81	1.75	1.68	1.63	1.91	1.96	1.76	1.78	1.75	1.73	1.79	1.91	1.96	1.97	1.99	1.81	1.75	1.81
Al_2O_3	14.75	14.84	14.56	14.61	14.45	14.71	14.52	14.38	14.64	14.51	14.61	14.56	14.79	14.77	14.31	14.35	14.21	14.62	14.41
FeO	21.51	21.38	21.71	21.52	21.12	20.98	21.19	20.99	21.37	20.97	20.91	21.38	21.01	21.32	20.56	20.44	20.83	20.11	20.91
MgO	10.55	10.85	10.96	10.96	10.86	10.84	10.85	11.15	11.35	11.22	11.12	11.01	10.98	11.01	11.36	11.24	11.55	11.81	11.15
MnO	0.21	0.23	0.21	0.28	0.31	0.33	0.35	0.25	0.34	0.37	0.31	0.33	0.27	0.23	0.31	0.35	0.33	0.21	0.25
K_2O	9.38	9.77	9.78	9.87	9.84	9.85	9.75	9.86	9.74	9.88	9.77	9.61	9.57	9.71	10.44	10.51	10.87	10.56	9.55
Total	95.00	94.85	95.78	95.43	94.82	94.79	94.98	94.93	95.57	95.11	95.01	95.19	95.24	95.78	95.6	94.96	96.13	95.27	94.49
Mg	0.4192	0.4541	0.4321	0.4541	0.4349	0.4541	0.4337	0.4541	0.4465	0.4541	0.4424	0.4541	0.4351	0.4541	0.4544	0.4541	0.4608	0.4541	0.444
Fe	0.4795	0.3897	0.4801	0.3897	0.4745	0.3897	0.4751	0.3897	0.4716	0.3897	0.4667	0.3897	0.467	0.3897	0.4614	0.3897	0.4662	0.3897	0.4671
Ti	0.0379	0.0287	0.0348	0.0287	0.0329	0.0287	0.0395	0.0287	0.0353	0.0287	0.0347	0.0287	0.0382	0.0287	0.0398	0.0287	0.0364	0.0287	0.0364
AlVI	0.0634	0.1276	0.053	0.1276	0.0577	0.1276	0.0517	0.1276	0.0466	0.1276	0.0561	0.1276	0.0597	0.1276	0.0444	0.1276	0.0366	0.1276	0.0525
K	1	0.9782	1	0.9782	1	0.9782	1	0.9782	1	0.9782	1	0.9782	1	0.9782	1	0.9782	1	0.9782	1
X_{Mg}	0.47	0.54	0.47	0.54	0.48	0.54	0.48	0.54	0.49	0.54	0.49	0.54	0.48	0.54	0.50	0.54	0.50	0.54	0.49

contain inclusion of titanite, Fe-oxides, apatite, biotite and zircon.

Fine-Grained Granite

Fine-grained granite occurs as enclaves in the biotite and biotite-amphibole granite (Fig. **3g**). This granite is fine-grained, dark-grey in color, and is made up of quartz (25-35 vol-%), K-feldspar (25-35 vol-%), plagioclase (8-15 vol-%), and biotite (5-12 vol-%).

Geochemistry

Representative major and trace element data for samples of granitoids of the magmatic complex of Bapa-Batié are listed in Table **5**.

Major Elements

In the QAPF diagram (Fig. **4**, [70]), the Bapa-Batié plutonic rocks fall in the granite and granodiorite fields. SiO_2 contents range from 68.87-72.89 wt% in biotite-granite and 70.23-74.74 wt% in biotite-amphibole-granite, 62.2-66.88 wt% in granodiorite and 69.07 to 72.16 wt% for fine-grained granite (syenogranite). Major element variations for Bapa-Batié plutonic rocks are shown on selected oxide diagrams (Fig. **5**). The biotite-granite samples show some slight chemical differences with other samples, in particular their much lower content of Na_2O, K_2O and Al_2O_3. The data for biotite-granite are well grouped except for K_2O which shows the least amount of scatter. SiO_2 is negatively correlated with Al_2O_3, MgO, Fe_2O_3, CaO, TiO_2 and P_2O_5. All granitoids have high total alkali contents (7 % < Na_2O+K_2O < 11%). They are K-rich, and transitional between the high-K calc-alkaline and the shoshonitic series (Fig. **6**). Their molar A/CNK ratios vary between 0.93 and 1.09 except for samples CM2 and CM7. Thus, all rocks are metaluminous (Debon and Lemmet, 1999), mildly peraluminous and correspond to I-type granite After Chappell and White

Table 4. Representative Analyses of Amphibole from Bapa-Batié Plutonic Rocks (wt%). Number of Ions on the Basis of 23 Oxygens

	Granodiorite											Biotite-Amphibole Granite							
N°	1	2	3	4	5	6	7	8	9	10	11	12	13	14	15	16	17	18	19
SiO_2	42.94	41.92	41.95	41.85	42.69	41.27	41.27	40.98	43.01	41.51	41.87	44.67	44.62	44.85	44.67	44.85	44.77	44.28	43.97
Al_2O_3	10.43	10.72	9.71	10.21	9.91	10.3	10.61	11.17	9.39	10.84	9.54	8.36	8.41	7.93	8.57	7.99	7.97	8.56	8.02
TiO_2	0.52	0.72	0.42	0.59	0.66	0.72	0.44	0.44	0.52	0.49	0.55	1.03	0.85	0.77	0.89	0.97	0.75	0.93	0.91
Fe_2O_3	5.82	5.71	6.31	6.06	5.39	6.28	6.66	6.46	5.89	6.45	6.43	5.37	5.42	5.43	5.12	4.96	5.31	4.61	6.45
FeO	16.33	16.18	17.21	16.54	16.74	16.68	15.25	15.91	15.25	15.72	15.26	13.49	13.45	13.53	13.35	13.94	13.41	14.01	12.91
MgO	7.37	7.27	7.66	7.87	7.83	7.85	9.14	7.87	8.95	7.91	9.91	10.5	10.61	10.81	10.65	10.75	10.88	10.98	11.12
CaO	11.33	11.95	11.51	11.59	11.56	11.71	11.61	11.67	11.65	11.67	11.69	11.61	11.65	11.61	11.82	11.65	11.69	11.51	11.53
Na_2O	1.37	1.36	1.21	1.24	1.39	1.28	1.57	1.39	1.36	1.41	1.34	1.46	1.34	1.39	1.28	1.47	1.28	1.55	1.51
K_2O	1.42	1.41	1.39	1.33	1.38	1.36	1.29	1.49	1.13	1.37	1.17	1.03	1.04	1.03	1.01	0.95	0.91	1.08	1.03
MnO	0.49	0.44	0.44	0.87	0.49	0.53	0.41	0.41	0.56	0.81	0.35	0.54	0.46	0.51	0.51	0.49	0.45	0.45	0.48
Cr_2O_3	0.05	0.02	0.06	0.04	0.04	0.04	0.06	0.06	0.13	0.07	0.14	0.03	0.03	0.02	0.05	0.04	0.05	0.05	0.05
Total	98.07	97.7	97.87	98.19	98.08	98.02	98.31	97.85	97.84	98.25	98.25	98.09	97.88	97.88	97.92	98.06	97.47	98.01	97.98
Si	6.8154	6.8171	6.7829	6.7715	6.775	6.7716	6.7641	6.8081	6.7626	6.7974	6.7199	6.715	6.7217	6.7128	6.7184	6.6949	6.7141	6.6847	6.7075
AlIV	1.1846	1.1829	1.2171	1.2285	1.225	1.2284	1.2359	1.1919	1.2374	1.2026	1.2801	1.285	1.2783	1.2872	1.2816	1.3051	1.2859	1.3153	1.2925
AlVI	2.0903	2.0928	2.0422	2.0253	2.0306	2.0256	2.0144	2.0796	2.0122	2.0637	1.949	1.9417	1.9516	1.9385	1.9467	1.9119	1.9404	1.8969	1.9306
Ti	0.0436	0.0604	0.0351	0.0492	0.055	0.06	0.0366	0.0369	0.0433	0.041	0.0455	0.0851	0.0703	0.0636	0.0736	0.0799	0.062	0.0765	0.0751
Fe^{3+}	0.4882	0.4791	0.5268	0.505	0.4494	0.5234	0.5544	0.5413	0.4902	0.5396	0.5318	0.4438	0.4484	0.4486	0.4234	0.4087	0.4388	0.3793	0.5325
Fe^{2+}	1.522	1.5084	1.5963	1.5316	1.5509	1.5446	1.4106	1.4812	1.4103	1.4612	1.4023	1.2387	1.2363	1.242	1.2265	1.2762	1.2312	1.2807	1.1842
Mg	1.2266	1.2102	1.2688	1.3014	1.2954	1.2981	1.5097	1.3084	1.478	1.313	1.6262	1.7218	1.7415	1.772	1.7472	1.7575	1.7838	1.7924	1.8214
Ca	0.5875	0.5877	0.5847	0.5837	0.584	0.5837	0.5831	0.5869	0.583	0.586	0.5793	0.5789	0.5794	0.5787	0.5792	0.5771	0.5788	0.5763	0.5782
Na	1.9114	1.9119	1.9023	1.8991	1.9001	1.8991	1.897	1.9094	1.8966	1.9063	1.8846	1.8832	1.8851	1.8826	1.8842	1.8776	1.883	1.8747	1.8811
K	0.0499	0.0499	0.0496	0.0495	0.0496	0.0495	0.0495	0.0498	0.0495	0.0497	0.0492	0.0491	0.0492	0.0491	0.0492	0.049	0.0491	0.0489	0.0491
Mn	0.0463	0.0416	0.0414	0.0817	0.046	0.0498	0.0385	0.0387	0.0525	0.0764	0.0326	0.0503	0.0429	0.0475	0.0475	0.0455	0.0419	0.0417	0.0446
Cr	0.0044	0.0018	0.0053	0.0035	0.0035	0.0035	0.0053	0.0053	0.0114	0.0062	0.0122	0.0026	0.0026	0.0017	0.0044	0.0035	0.0043	0.0043	0.0043
Al	3.2749	3.2758	3.2593	3.2538	3.2556	3.2539	3.2503	3.2715	3.2496	3.2663	3.2291	3.2267	3.2299	3.2257	3.2283	3.217	3.2263	3.2122	3.2231
Name and classification after Leake et al. (1997)																			
(Ca)B	0.5875	0.5877	0.5847	0.5837	0.584	0.5837	0.5831	0.5869	0.583	0.586	0.5793	0.5789	0.5794	0.5787	0.5792	0.5771	0.5788	0.5763	0.5782
(Na)B	1.4125	1.4123	1.4153	1.4163	1.416	1.4163	1.4169	1.4131	1.417	1.414	1.4207	1.4211	1.4206	1.4213	1.4208	1.4229	1.4212	1.4237	1.4218
(Ca + Na)B	2	2	2	2	2	2	2	2	2	2	2	2	2	2	2	2	2	2	2
(Na)A	0.4989	0.4995	0.487	0.4828	0.4841	0.4829	0.4801	0.4963	0.4795	0.4923	0.4639	0.4621	0.4645	0.4613	0.4633	0.4547	0.4618	0.451	0.4594
(K)A	0.0499	0.0499	0.0496	0.0495	0.0496	0.0495	0.0495	0.0498	0.0495	0.0497	0.0492	0.0491	0.0492	0.0491	0.0492	0.049	0.0491	0.0489	0.0491
(Na + K)A	0.5488	0.5494	0.5366	0.5323	0.5337	0.5324	0.5296	0.5461	0.529	0.542	0.5131	0.5112	0.5137	0.5104	0.5125	0.5037	0.5109	0.4999	0.5084
$Mg/(Mg+Fe^{2+})$	0.4463	0.4452	0.4428	0.4594	0.4551	0.4566	0.517	0.469	0.5117	0.4733	0.537	0.5816	0.5848	0.5879	0.5876	0.5793	0.5916	0.5832	0.606
	Katop	Katop	Katop	Katop	Katop	Katop	MgKatop	Katop	MgKatop	Katop	MgKatop	MgKatop	MgKatop	MgKatop	MgKatop	MgKatop	MgKatop	MgKatop	MgKatop
Katop = Katophorite MgKatop = Magnesio -katophorite																			

(1974). The high K_2O contents of the biotite-granite (3.93-6.63%), biotite-amphibole-granite (3.92-6.01%), granodiorite (5.23-6.25) and fine-grained granite (5.8 to 6.63%) are especially worth noting. All the rocks form a ferriferous type association (Fe* > 0.73; Fig. **7**; [32, 33]).

Trace Elements

Trace element concentrations of the Bapa-Batié rocks are listed in Table **5**. Selected elements are plotted against SiO_2 content in Fig. (**8**). Ba, Sr, Y, Zr, and Co concentrations decrease with increasing SiO_2 content. Cr, Ni, Zn and Rb concentrations are in general scattered on variation diagrams. Ba/Sr ratios range between 2.5-5.9 and Ba/Rb between 0.9-18.3; Zr/Nb and Zr/Y ratios are between 3-47.4 and 8.2 to 40.4 respectively. These values are similar to those observed in continental calc-alkaline igneous suites (e.g. [34, 35]). Some features are noteworthy. The plutonic rocks of Bapa-Batié complex show a large scatter of data for Ba (349-2739ppm), Cr (43-229ppm), Nb (5-30ppm), Rb (98-784ppm) and Sr (98-609ppm). Ba abundance is high in the granodiorite (762-2739 ppm) and moderate in biotite-amphibole-granite (565-1140 ppm).

Total REE concentrations are higher (179-533ppm) in biotite-granite and fine-grained granite (377-640ppm) compared to the biotite-amphibole-granite (127-269ppm) and the granodiorite (136-303ppm). Chondrite-normalized rare earth element (REE) patterns of the Bapa-Batié suite (Fig. **9**) resemble each other, in general with a strong LREE enrichment with La_N/Yb_N ratios of 8-80 and Gd_N/Yb_N ratios of 1-10. Negative Eu* anomalies are pronounced in the biotite-granite (Eu/Eu* = 0.25-0.46) and the biotite-amphibole-granite (Eu/Eu* = 0.42-0.58) whereas they are not significant in the granodiorite (Eu/Eu* = 0.79-1.05), and moderate (Eu/Eu* = 0.96-1.0) to positive (Eu/Eu* = 1.08-1.32) in the fine-grained granite, indicating enrichment of europium relative to the neighbouring REE (Fig. **9g**). The multi-element spectra (Fig. **9b**, **d**, **f**, **h**) of all these rocks show a distinctive depletion in Nb, Sr, P, Ti and Y relative to other trace elements; they are enriched in LILE (large ion lithophile elements) and display negative anomalies in Sr, Ba and Ti. Distinctively higher contents of Th are observed in the biotite- granite and fine-grained granite. These rocks display less pronounced negative anomalies in Sr and Ti, and lower Rb, Y and Yb values resulting in more "fractionated" trace element distribution patterns, characteristic of calc-alkaline arc granitoids. Overall, the enrichment in the

Table 5. Representative Chemical Analyses of Bapa-Batié Plutonic Rocks (wt%)

Sample	CM1	CM2	CM3	CM5	CM6	CM7	Biotite Granites CM11'	CM11''	CM12	B4	B5	B7	B9	B11	B13	B15	B16	CM8	B1	B3	Biotite-Amphibole Granites B10	B14	B18	CM2b	M1	Quartz Syenites M1b	M3	M5	B2	Fine-Grained Granites B6	B8	B12	B17
Rocks																																	
SiO_2	72.74	72.89	71.48	69.97	70.14	72.91	70.26	72.27	70.88	69.61	70.76	70.5	71.46	72.8	72.82	72.41	68.87	69.73	74.74	70.59	71.54	71.69	70.23	71.93	66.88	65.75	64.18	62.2	65.1	70.7	69.07	70.4	71.05	72.16
TiO_2	0.35	0.31	0.42	0.54	0.51	0.32	0.32	0.35	0.39	0.31	0.34	0.4	0.39	0.34	0.39	0.33	0.38	0.54	0.16	0.31	0.26	0.29	0.26	0.37	0.52	0.80	0.82	0.93	0.78	0.4	0.55	0.49	0.42	0.4
Al_2O_3	13.74	14.32	13.49	13.90	13.88	14.70	14.64	13.64	14.55	14.51	15.12	14.24	14.84	13.84	13.72	14.82	16.21	14.07	13.10	14.57	14.31	14.21	15.12	14.22	15.23	15.52	15.68	16.12	16.83	14.33	15.2	14.55	14.33	13.78
Fe_2O_3*	2.17	2.02	2.62	3.17	2.99	2.26	2.15	2.28	2.33	1.87	2.51	2.74	2.79	1.95	2.71	2.24	2.55	2.85	1.73	2.69	2.41	2.41	2.21	2.8	3.51	3.93	4.50	4.97	3.59	2.64	3.84	3.29	3.06	2.81
MnO	0.04	0.03	0.04	0.06	0.05	0.03	0.06	0.05	0.05	0.04	0.03	0.04	0.03	0.03	0.03	0.03	0.02	0.03	0.06	0.01	0.04	0.04	0.04	0.05	0.06	0.05	0.06	0.10	0.09	0.03	0.06	0.03	0.05	0.03
MgO	0.43	0.39	0.58	0.62	0.59	0.52	0.42	0.44	0.43	0.35	0.31	0.36	0.03	0.03	0.03	0.03	0.02	0.03	0.19	0.24	0.25	0.04	0.04	0.05	1.17	1.15	1.48	1.63	0.92	0.39	0.66	0.03	0.05	0.03
CaO	1.49	1.11	1.58	1.63	1.65	1.28	1.47	1.53	1.44	1.36	1.2	1.28	1.22	1.06	1.38	1.27	1.2	1.51	1.31	1.11	1.14	1.21	2.18	1.25	2.39	2.12	2.52	2.88	1.82	1.41	1.79	1.51	1.23	1.32
Na_2O	3.87	3.02	3.51	2.97	3.04	3.01	4.58	2.93	2.87	3.00	3.73	3.71	3.18	3.26	3.41	3.46	3.66	3.13	3.81	3.6	3.58	3.78	3.64	3.81	3.49	3.48	3.52	4.09	4.24	3.29	3.88	3.32	3.62	3.48
K_2O	3.93	4.51	4.45	5.63	5.57	4.86	4.45	6.01	6.9	6.55	5.78	5.61	5.48	5.82	5.02	5.17	6.63	5.52	3.92	6.01	5.92	5.44	5.5	5.33	5.26	5.67	5.42	5.23	6.23	6.63	5.13	5.51	5.85	5.18
LI	0.32	0.31	0.51	0.51	0.49	0.86	0.56	1.50	0.92	1.45	0.04	0.6	0.35	0.55	0.21	0.11	0.11	0.21	0.20	0.6	0.35	0.44	0.11	0.21	0.48	0.50	0.58	0.71	0.62	0.03	0.04	0.43	0.11	0.22
P_2O_5	0.13	0.13	0.15	0.19	0.18	0.10	0.13	0.12	0.14	0.11	0.18	0.13	0.13	0.1	0.11	0.13	0.16	0.17	0.05	0.1	0.1	0.12	0.1	0.12	0.18	0.26	0.30	0.32	0.21	0.16	0.22	0.15	0.15	0.11
Total	99.21	99.04	98.83	99.19	99.09	100.85	99.04	99.91	100.01	99.16	100	99.61	99.9	99.78	99.83	100	99.81	97.79	99.27	99.83	99.9	99.67	99.43	100.14	99.17	99.23	99.06	99.18	100.43	100.01	100.44	99.71	99.92	99.52
A/CNK	1.0	1.2	1.0	1.0	1.0	1.2	1.0	1.0	1.0	1.0	1.0	1.0	1.1	1.0	1.0	1.1	1.1	1.0	1.0	1.0	1.0	1.0	0.9	1.0	1.0	1.0	1.0	0.9	1.0	0.9	1.0	1.0	1.0	1.0
Rb	251	255	258	265	258	210	362	302	784	412	356	268	312	339	224	331	363	211	177	294	320	330	121	336	98	144	150	150	129	251	287	279	331	218
Sr	122	116	156	206	216	98	111	140	180	163	152	162	140	141	130	150	177	186	152	130	126	135	300	161	309	496	570	609	347	198	180	177	147	150
Ba	349	443	538	707	708	433	321	534	687	756	814	666	627	541	496	565	853	765	897	634	565	592	1140	609	762	1737	1659	2739	2039	894	671	733	696	562
Y	20	23	16	22	19	17	12	18	17	17	10	8	14	14	4	11	9	7	27	5	6	8	13	10	12	16	17	25	29	7	8	22	25	9
Zr	182	186	222	315	276	217	117	174	175	219	249	237	224	161	218	164	225	283	117	115	173	179	111	156	302	287	276	283	344	229	310	298	240	265
V	17	20	28	27	27	19	18	22	26	22	18	18	17	21	21	23	21	23	11						31	45	52	64	27					
Nb	30	24	28	28	27	18	31	33	58	30	8	5	12	6	6	8	10	6	11	7	5	8	6	21	9	16	16	16	20	6	16	8	11	6
Cr	70	115	63	81	71	68	102	131	229	116	125	158	191	178	171	165	157	49	61	134	122	167	156	120	59	43	53	58	94	150	141	189	136	144
Ni	3	2	4	7	4	3	4	5	9	14	4	4	4	4	4	4	3	10	2	4	4	4	8	21	4	8	7	9	5	4	4	4	4	3
Cu	23	5	11	6	5	6	8	9	15	10	6	7	6	7	8	8	9	7	5						6	6	4	2	7					
Zn	314	223	198	191	210	197	271	142	171	141	158	154	170	143	144	145	157	151	140	32	44	49	25	48	34	42	48	63	155	49	80	57	54	43
Ga	28	36	46	38	50	36	33	39	89	52	28	33	31	27	29	30	31	30	50						45	70	70	102	105					
Be	6	4	5	5	5	3	12	6	5	6	3	3	6	6	7	7	7	6	6						2	3	3	5	3					
Sc	5	5	6	5	5	5	6	6	12	5	6	6	3	4	5	5	7	5	6						5	9	11	11	9					
Co	3	3	4	4	4	4	3	3	3	3	2	3	3	2	2	4	3	4	1	1.18	1.21	1.16	1.112	1.1087	4	6	7	8	5	5.21	5.198	6.921	5.456	5.209
La	64.131	65.837	84.122	110.112	100.832	86.472	33.325	77.461	63.197	70.394	70.234	117.121	128.372	86.297	122.110	78.737	117.130	112.120	23.831	39.000	36.490	40.000	20.000	49.000	28.350	66.271	70.744	61.507	61.095	104.000	141.000	158.000	153.000	184.000
Ce	129.430	130.811	162.631	221.627	201.189	158.716	66.462	152.467	136.988	133.921	137.211	178.010	200.270	117.190	195.110	115.810	163.810	151.091	45.688	73.000	119.000	77.000	73.000	110.000	54.016	118.932	122.503	122.196	131.199	148.000	214.000	235.000	218.000	278.000
Pr	13.977	13.833	17.421	23.945	21.444	17.032	7.431	16.527	17.153	14.275	15.132	16.311	16.010	18.010	19.630	21.070	22.312	22.837	5.346	7.236	8.560	8.023	6.982	6.015	5.833	12.178	12.917	13.431	15.241	10.220	12.340	11.980	10.582	12.084
Nd	48.303	49.302	57.710	83.420	73.979	58.863	26.273	55.635	56.459	49.182	36.459	54.627	61.120	47.937	48.130	35.183	55.307	48.991	20.961	24.000	37.000	24.000	23.000	27.000	20.890	41.845	44.643	53.015	58.530	48.000	77.000	60.000	74.000	70.000
Sm	9.618	8.666	9.929	12.646	11.599	9.634	4.765	9.674	13.654	8.548	5.370	6.987	9.371	9.991	10.121	10.234	12.012	8.887	4.323	4.377	5.990	5.137	5.781	4.997	3.588	6.468	7.297	9.040	10.950	8.044	12.214	11.982	12.094	12.736
Eu	0.731	0.783	0.790	1.299	1.163	0.777	0.621	0.811	1.127	0.938	0.719	0.699	0.787	0.923	1.001	0.821	0.789	0.701	0.840	0.809	0.890	0.831	0.736	0.879	0.731	1.828	1.953	2.406	2.403	3.025	3.250	3.115	3.487	3.977
Gd	5.942	6.158	5.899	8.136	6.940	5.961	3.536	6.466	8.599	5.941	4.997	5.347	6.198	5.987	6.597	6.877	8.012	7.123	4.543	4.124	3.967	4.032	4.902	4.873	2.625	4.396	5.093	6.552	7.906	6.082	8.098	8.234	8.008	7.998
Tb	0.785	0.811	0.784	0.939	0.828	0.720	0.453	0.868	0.933	0.783	0.876	0.881	0.801	0.789	0.821	0.812	0.437	0.567	0.696	0.496	0.500	0.500	0.431	0.504	0.373	0.497	0.610	0.863	0.993	0.776	1.001	0.993	1.012	1.232
Dy	4.013	4.556	3.843	4.735	4.250	3.862	2.122	4.068	3.452	3.828	3.789	4.012	4.230	3.890	3.989	4.576	4.354	4.324	4.724	4.213	3.180	3.965	4.541	4.932	2.067	3.076	3.542	4.857	5.948	5.206	6.706	7.002	7.262	7.835
Ho	0.652	0.808	0.567	0.775	0.691	0.583	0.366	0.611	0.516	0.581	0.687	0.415	0.579	0.697	0.675	0.541	0.554	0.345	0.942	0.378	0.380	0.401	0.369	0.411	0.407	0.606	0.614	0.892	1.036	0.998	1.046	1.076	1.118	1.098
Er	1.682	1.872	1.505	1.966	1.731	1.557	0.960	1.553	1.159	1.530	1.481	1.531	1.640	1.750	1.981	1.781	1.650	1.961	2.686	2.132	1.010	1.986	1.873	2.009	1.145	1.422	1.616	2.447	2.623	1.689	2.763	2.984	2.874	2.833
Tm	0.199	0.237	0.196	0.257	0.245	0.192	0.125	0.191	0.153	0.216	0.195	0.213	0.224	0.194	0.233	0.215	0.224	0.201	0.444	0.330	0.120	0.220	0.180	0.160	0.153	0.192	0.239	0.323	0.331	0.243	0.350	0.344	0.354	0.367
Yb	1.491	1.492	1.170	1.505	1.467	1.202	0.964	1.124	0.685	1.135	1.121	1.203	1.510	1.271	1.203	1.124	0.987	1.341	2.809	0.809	0.660	0.709	0.901	0.876	1.121	1.440	1.756	2.235	2.429	1.860	2.860	2.874	2.978	2.998
Lu	0.215	0.186	0.148	0.232	0.191	0.164	0.174	0.144	0.141	0.188	0.150	0.160	0.201	0.192	0.186	0.18	0.109	0.211	0.454	0.345	0.110	0.160	0.180	0.108	0.176	0.222	0.233	0.362	0.371	0.246	0.390	0.422	0.412	0.402
Hf	5.520	5.595	6.915	8.229	7.302	6.121	3.781	4.737	5.866	6.300	7.768	7.861	8.008	8.932	6.998	8.654	6.476	6.896	3.142	3.092	2.084	2.644	2.872	2.988	2.661	7.233	7.391	7.016	8.386	7.001	8.009	7.997	7.876	8.362
Ta	2.028	1.402	1.516	1.626	1.515	0.727	3.399	1.674	2.625	1.515	2.160	2.224	2.345	3.001	2.964	2.764	2.563	2.334	1.208	1.010	0.998	1.180	1.080	1.104	1.115	1.088	1.071	1.086	1.112	1.086	1.234	1.312	1.322	1.032
Pb	25.080	25.307	25.547	24.720	24.543	14.867	24.211	26.724	71.587	38.776	13.000	7.000	8.000	16.000	6.000	10.000	16.000	6.000	11.137	12.000	13.000	15.000	6.000	10.000	14.986	23.942	23.405	24.221	23.764	10.000	10.000	9.000	11.000	6.000
Th	42.838	44.983	57.209	51.827	47.149	63.799	24.081	46.318	51.242	49.551	27.000	49.000	41.000	37.000	36.000	24.000	38.000	24.000	4.029	14.000	48.000	36.000	6.000	21.000	10.431	14.141	13.774	14.505	8.706	31.000	69.000	63.000	55.000	45.000
U	4.406		4.525	5.504	4.709	8.598	7.226	7.410	9.118	8.685	9.000	10.000	8.000	10.000	9.000	10.000	11.000	9.000	5.347	11.000	9.000	8.000	8.000	11.000	2.574	2.626	2.310	3.315	2.368	11.000	10.000	9.000	9.000	10.000
(La/Yb)N	29.032	29.791	48.516	49.395	46.394	48.545	23.326	46.531	62.242	41.863	42.289	65.692	57.372	45.847	68.496	47.304	80.077	56.439	8.1283	14.552	11.403	11.208	10.652	17.63	17.075	31.056	27.189	18.573	16.98	37.741	33.277	37.107	34.678	41.426
(Gd/Yb)N	3.2206	3.3363	4.0731	4.3697	3.823	4.0063	2.9635	4.6503	10.14	4.2298	3.6023	3.5907	3.3164	3.8081	4.4305	4.9466	6.558	4.2928	1.3067	1.8423	1.4842	1.3525	2.0837	2.0991	1.8927	2.4663	2.3434	2.3688	2.6306	2.6425	2.2882	2.3153	2.1731	2.1559
Eu/Eu*	**0.2956**	**0.3278**	**0.3155**	**0.3914**	**0.3962**	**0.3133**	**0.4625**	**0.3134**	**0.3179**	**0.4023**	**0.4243**	**0.3496**	**0.3157**	**0.3648**	**0.3745**	**0.2992**	**0.2459**	**0.2694**	**0.5792**	**0.5821**	**0.5582**	**0.5582**	**0.4227**	**0.5446**	**0.7279**	**1.0479**	**0.9792**	**0.9559**	**0.7895**	**1.32**	**1.00**	**0.96**	**1.08**	**1.20**

incompatible elements (K, Rb, and Ba) and depletion in high field strength elements (HFSE) supports the importance of the crustal source component in the genesis of the Bapa-Batié granitoids. Thus the overall distribution of major and trace elements observed is typical of those of calc-alkaline rocks.

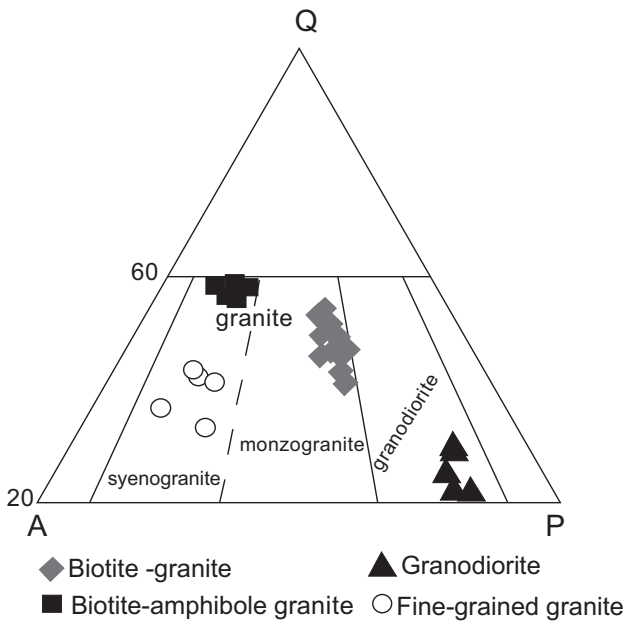

Fig. (4). Position of the Bapa-Batié granitoids in the QAPF diagram.

Summarily, the geochemical variations confirm the presence of four distinct types of plutonic rocks within the Bapa-Batié area. These plutonic rocks are metaluminous, high-K calc-alkaline ferro-potassic in composition. They have petrographical and geochemical characteristics of I-type rocks. Each plutonic group is characterized by specific magmatic evolution trend on the geochemical variation diagrams.

In terms of major and trace elements, some features are common to all plutons of the Bapa-Batié, eastern Nigeria [36-38] and Borborema Province in the NE Brazil [39-43]: (1) the rocks are high-K calc-alkaline to shoshonitic associations (Fig. **10a**); (2) they are also metaluminous to weakly peraluminous (Fig. **10b**); (3) silica contents typically > 50 wt%; (4) the enrichment in the incompatible elements (K, Rb, and Ba) and depletion in high field strength elements (HFSE). Although one difference between the studied plutons, eastern Nigeria plutons and those of the Borborema Province in the NE Brazil are apparent in Fig. (**10c**), the Bapa-Batié and eastern Nigeria plutons form a ferriferous type association while the plutons of the Borborema Province in the NE Brazil are magnesian.

Zirconium Saturation Geothermometry

Pearce (1982) [44], Harrison and Watson (1983) [45], Watson and Harrison (1983) [46] demonstrated that the Zr contents of igneous rocks would be inherited from their source rocks and controlled by degree of partial melting involved during their generation; high Zr contents correspond to higher degrees of partial melting for the same source rock. Granitoids from the Bapa-Batié area could come from similar source rocks, and their Zr distributions could be ascribed to quite different degrees of partial melt of that source rock.

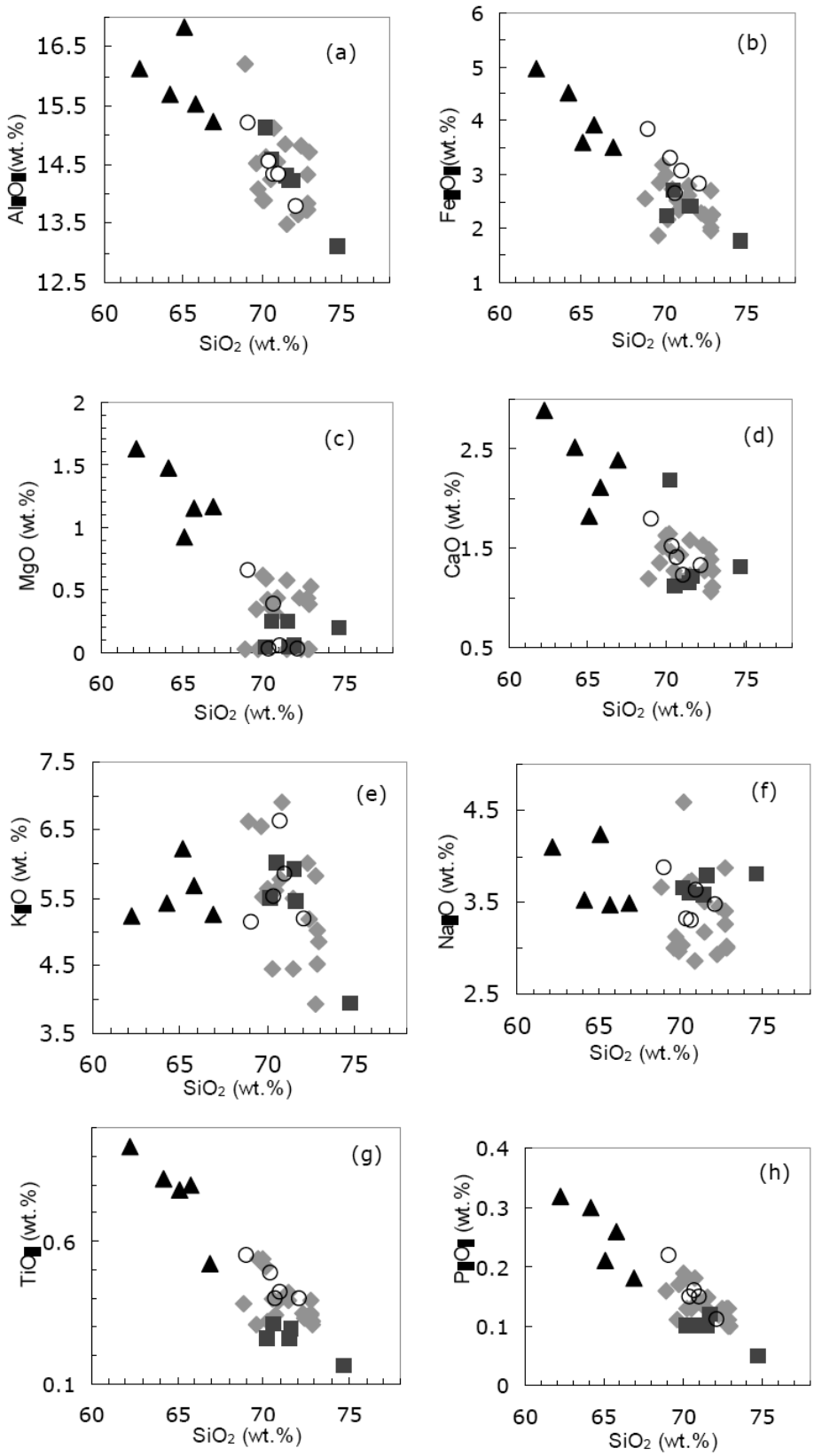

Fig. (5). Harker diagrams of selected major elements. Symbols as in Fig. (**4**).

We applied the Zr saturation geothermometer [45, 46] to the Bapa-Batié granitoids to estimate the minimum temperatures of the melts (assuming that there is no residual zircon inherited from the source). The calculated temperatures (Table **6**) range between 749-839ºC for the biotite granite, 741-789°C for the amphibole-biotite granite, 801-834°C for the granodiorite and 802- 838°C for the fine-grained granite.

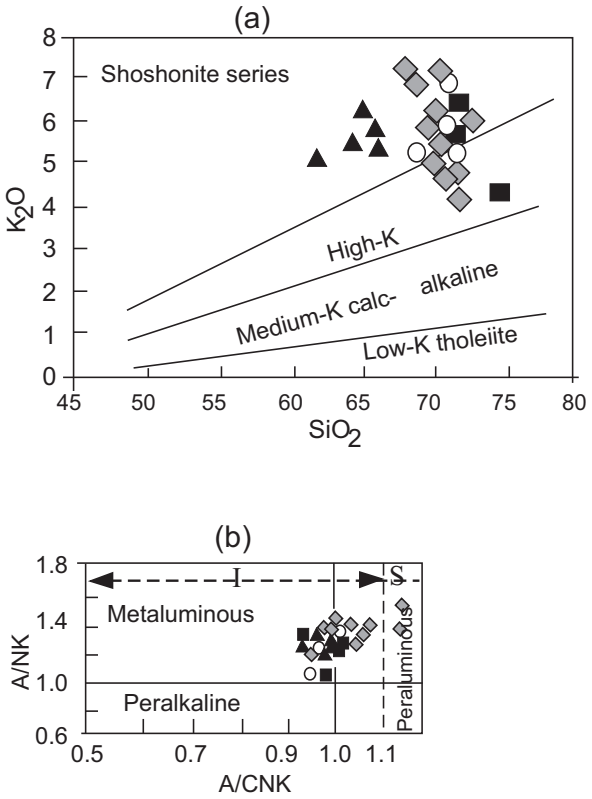

Fig. (6). (**a**) SiO_2 *vs* K_2O diagram showing high-K calc-alkaline and shoshonitic Affinity of the Bapa-Batié granitoids After [71, 72]: dotted line. (**b**) A/NK *vs* A/CNK diagram showing metaluminous weakly peraluminous character of the Bapa-Batié granitoids.

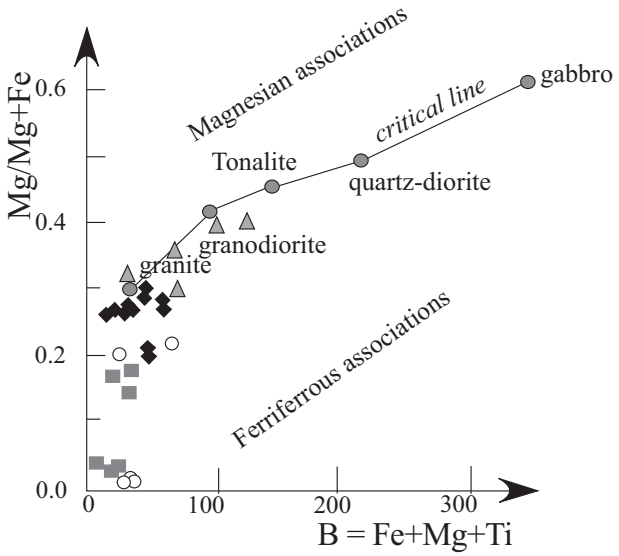

Fig. (7). Mg/Mg + Fe diagram of Debon and Lemmet (1999) [32]. Symbols as in Fig. (**4**).

Zircon U-Pb Data

The most common textural features include bands parallel to the prism faces oscillatory zoning, typical of growth in magmatic conditions. All analytical points are concordant and overlap nicely on the Concordia curve for each sample, using the software Isoplot/Ex [31] at 95% confidence level.

Zircon grains of biotite- granite (sample Batié) and biotite- amphibole granite (sample CM8) are elongated with euhedral to subhedral shape; oscillatory zoning, typical of magmatic growth, is common (Fig. **11**). Tables **7** and **8** show the results of analytical data for the studied samples. The zircon grains plot close to Concordia (Fig. **12**) at 600 ± 3.7 Ma (MSWD = 2.1) and 619 ± 19 Ma (MSWD = 0.23). The high concordance of zircon grains and the typical magmatic growth indicate that these ages of 600 Ma and 619 Ma are those of the crystallization of the zircons in the biotite-amphibole granite and biotite- granite, respectively, and also correspond to the age of emplacement during the Pan-African orogeny.

DISCUSSION

Constraints on the Source of the Bapa-Batié Plutonic Rocks

The investigated plutonic rocks exhibit petrographical and chemical compositions characteristic of high-K to shoshonitic I-type granitoids [47, 48] derived from partial melting of igneous protoliths. From the several studies carried out to constrain the generation of high-K magmas in convergent tectonic settings, two main processes are commonly recognized [49]: (i) in continental arc settings, parent mantle melts that are enriched in slab-derived fluids may become contaminated with crustal material during ascent [50]; (ii) in syn- to post-collisional settings, crustal source rocks may occur as a consequence of decompression following delamination of the lithospheric root or slab breakoff (e.g. [51, 52]). The geochemical compositions of Bapa-Batié granitoids as shown on Harker´s diagrams did not indicate continuous compositional variation from one group to another but little internal compositional variation and overlap between some groups. This suggests that the compositional variability of these granitoids does not appear to be generated mainly by fractionation processes but probably reflects the primary compositions of anatectic melts generated at various crustal levels. The nature of the igneous source can be constrained using the geochemical signatures of the plutonic rocks. The REE and multi-element patterns (Fig. **9**) suggest genetic processes involving garnet. The high contents of LREE in all rocks could be related either to the enrichment of their source materials in LREE, or to a low degree of partial melting of source protoliths with garnet and amphibole among the residual phases. However, their concentrations in HREE (more or less 10 times the chondrite values) do not support the assumption of a source containing garnet. Moreover, the spider diagrams (Fig. **9**) show negative anomaly in Y, suggesting that garnet was involved in the residual phase. The spider diagrams characteristically display negative anomalies for Ba, Nb, Sr, P, Ti and Y. As explained above, concentration of elements in a melt derived by partial melting depends upon both the content of these elements in the source and their retention in the residue during partial melting. The geochemistry and mineralogy of the granitic rocks reflect not only the nature of the protoliths from which they were derived, but also the dynamic conditions under which magmas were formed, evolved and eventually solidified [53]. Compositional differences of melts produced by partial melting of different source rocks, such as amphibolites, tonalitic gneisses, metapelites and

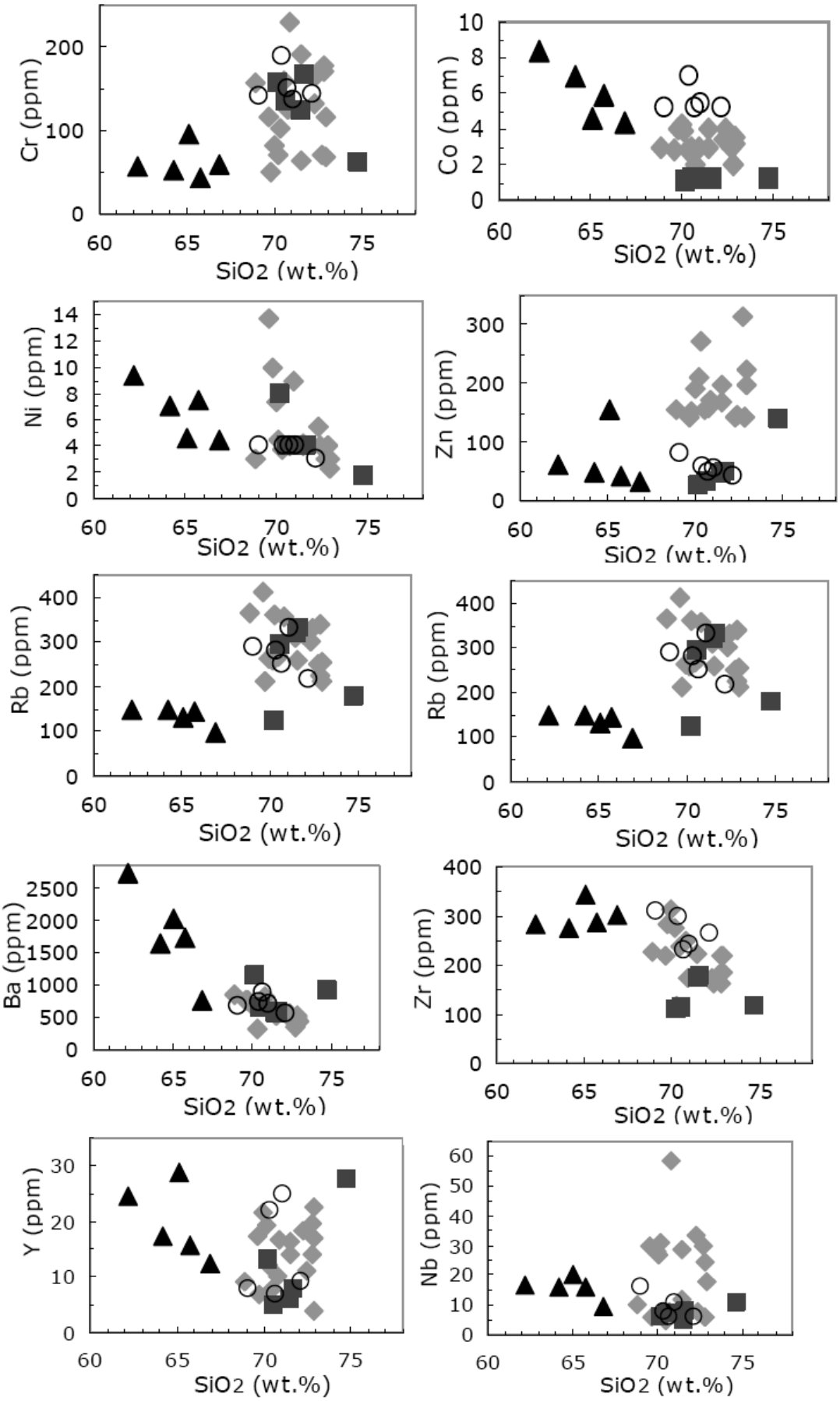

Fig. (8). Harker diagrams of selected trace elements. Symbols as in Fig. (**4**).

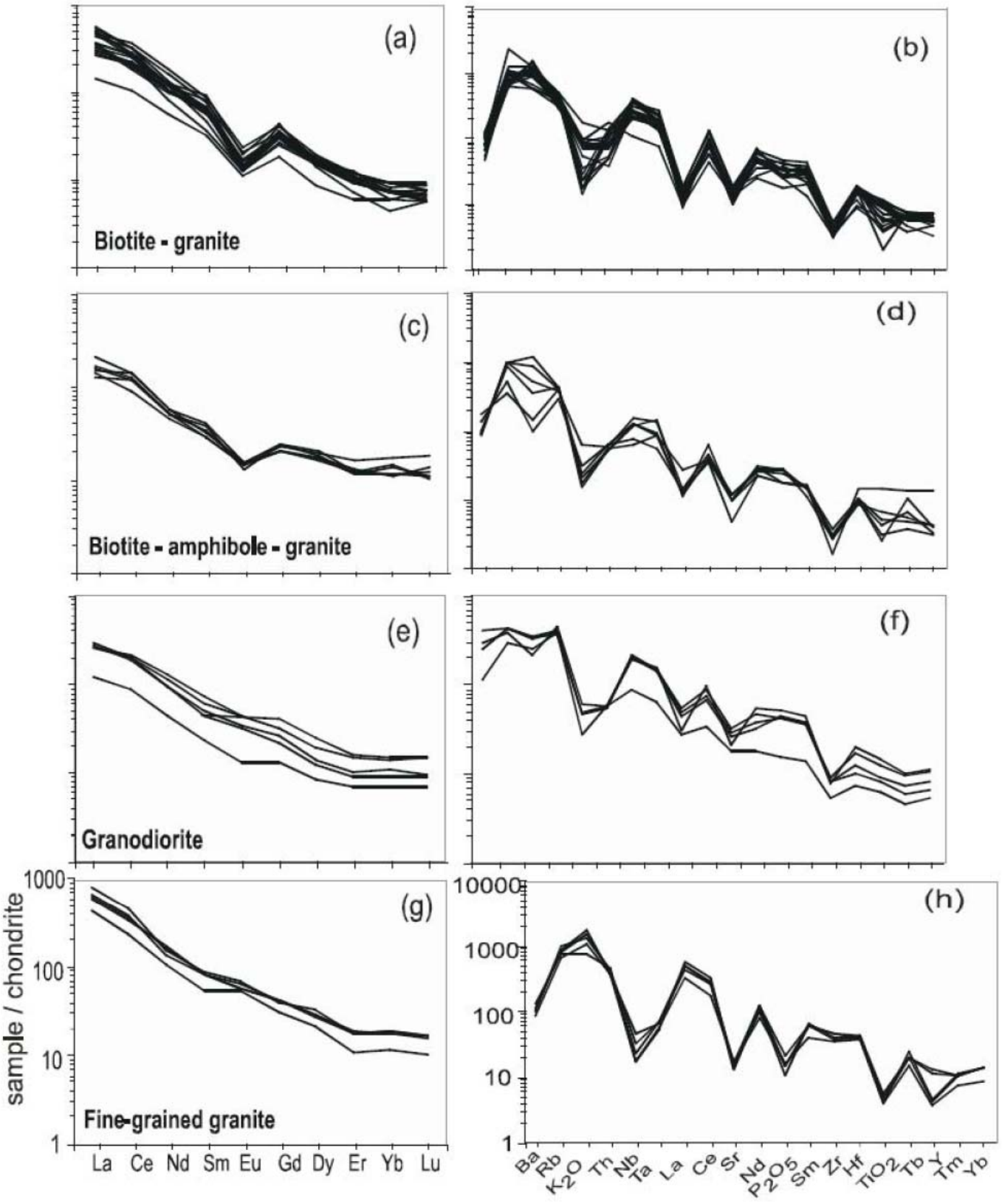

Fig. (9). Chondrite-normalised REE patterns for the Bapa-Batié granitoids. The normalizing values are from [73].

(**a**)

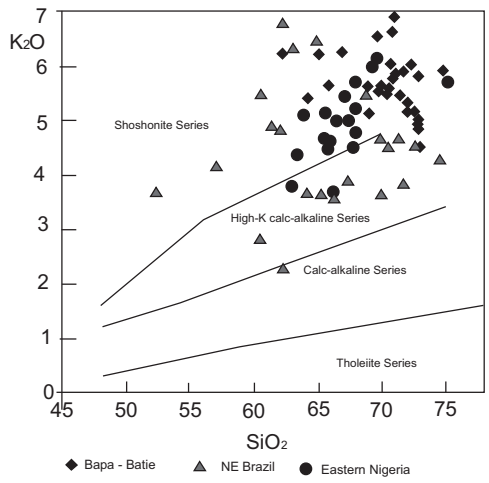

(**b**)

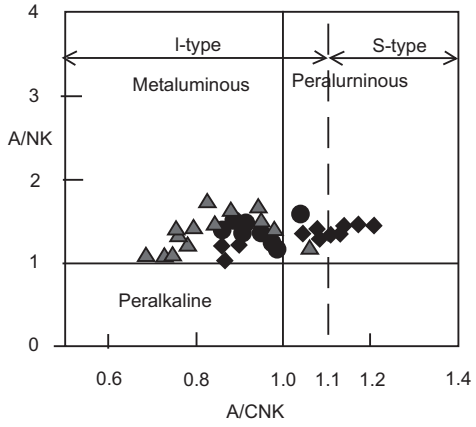

(**c**)

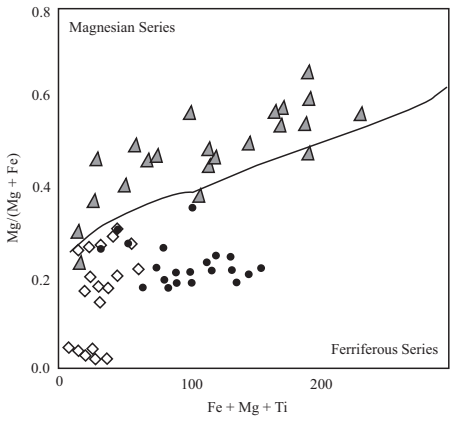

Fig. (10). (**a**) SiO_2 *vs* K_2O and (**b**) A/NK *vs* A/CNK diagrams showing the same high-K calc-alkaline and shoshonitic Affinity, metaluminous weakly peraluminous character of the Bapa-Batié granitoids, Borborema province in NE Brazil granitoids [40, 41] and eastern Nigeria granitoids [37, 38]. (**c**) Magnesian associations of NE Brazil granitoids different for those ferriferous of Bapa-Batié and eastern Nigeria granitoids.

Table 6. Estimate of the Minimum Temperature of the Melts of the Bapa-Batié Granitoids with the Zirconium Saturation Geothermometry [45, 46]

Sample	Zr (ppm)	Temperature (°C)
CM1	182	796
CM2	186	815
CM3	222	810
CM5	315	839
CM6	276	826
CM7	217	825
Batie	117	749
CM11a	174	784
CM11b	175	784
CM12	219	806
B4	249	821
B5	237	811
B7	224	821
B9	161	784
B11	218	810
B13	164	792
B15	225	810
B16	283	832
CM8	117	760
B1	115	751
B3	173	785
B10	179	789
B14	111	741
B18	156	777
CM2b	302	825
M1	287	820
M1b	276	811
M3	283	801
M5	344	834
B2	229	802
B6	310	834
B8	298	838
B12	240	813
B17	265	827

metagreywackes, under variable melting conditions can be visualized in terms of molar $CaO/(MgO + FeO_{total})$ *vs* molar $Al_2O_3/(MgO + FeO_{total})$ ([49]; Fig. **13**). In that diagram, most of the samples plot in the field of partial melts from

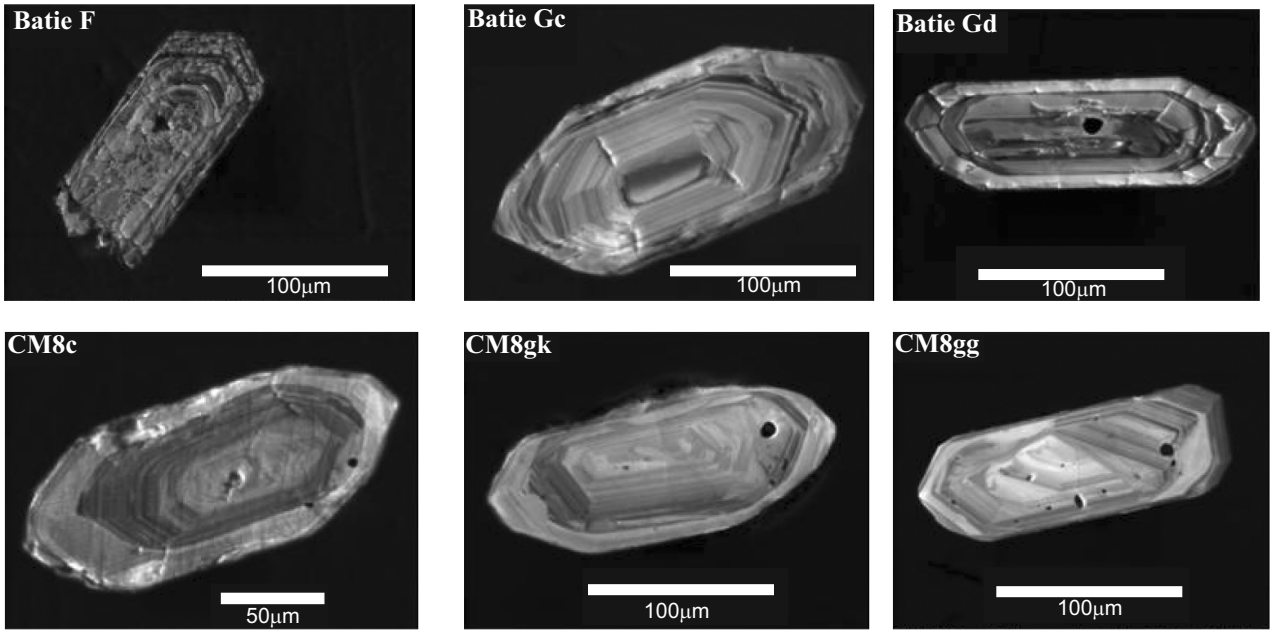

Fig. (11). SEM images of selected dated zircon grains in biotite- granite (sample Batié) and biotite-amphibole granite (sample CM8) showing oscillatory zoning, typical of magmatic growth.

metagreywacke sources. These source rocks are predominantly found in the upper part of the continental crust and we suggest that the source for the Bapa-Batié plutonic rocks was metamorphosed metagreywackes rocks. Presence of garnet in the residual phase requires that the partial melting process occurred at pressure higher than 5 kb (e.g. [54, 55]). Such source protolith with significant proportions of metasedimentary rocks was indicated for the high-K calc-alkaline plutons of the Borborema province in the NE Brazil [40, 41, 56, 57] and eastern Nigeria [36, 38, 58]. The high-K calc-alkaline to shoshonitic and metaluminous nature of the Bapa-Batié plutonic rocks require a metaluminous and relatively K-rich source [51, 59]. The differences observed in granites can be explained by differences in melting conditions and/or minor variation in source compositions. The low Rb/Sr and the enrichment of LREE of the rocks are probably inherited from the source. Thus, the magmatism of the Bapa-Batié plutonic rocks may have involved remelting of a composite acid metagreywacke protolith in the upper crust. The low Ni and relative high Cr contents of the rocks are consistent with such a model. The large-scale melting of the source rocks could have been favoured by high heat flow during Pan-African orogenesis or underplating of mantle-derived magmas into the crust.

Petrogenesis

Field relations, petrographical features, whole rock major and trace element geochemistry are inconsistent with the derivation of the Bapa-Batié plutonic rocks from a common parental magma by simple crystal fractionation processes. Rather metasedimentary rocks are suggested as protoliths for these granitoids. As seen in Table **5**, concentrations of Zr are high (117 to 315 ppm in biotite- granite, 111 to 156 ppm in biotite-amphibole granite, 276- 344 ppm in granodiorite and

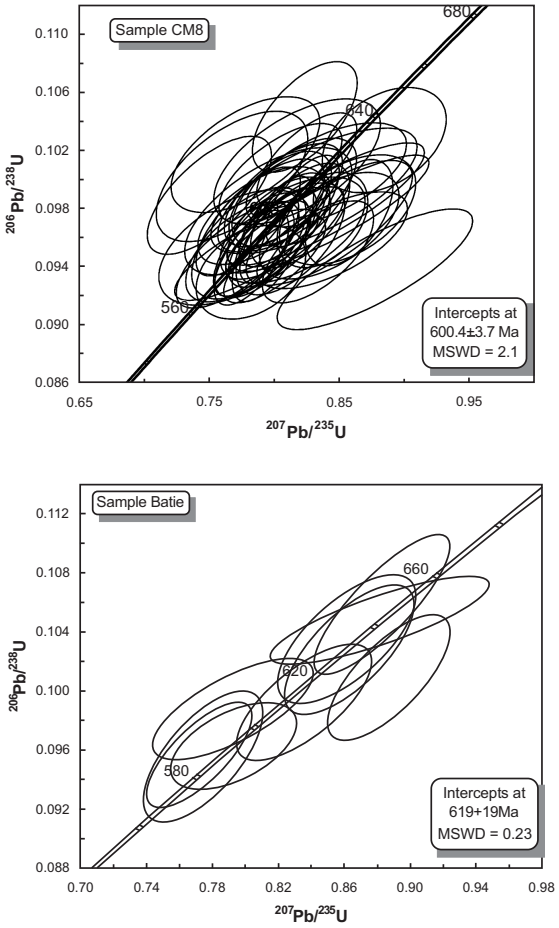

Fig. (12). U-Pb Concordia diagram for zircons from samples Batié and CM8.

Table 7. LA-ICP-MS U-Pb Results for Zircons from Biotite- Granite of the Bapa-Batié Area

	Isotopic Ratios				Apparent Ages (Ma)					
Sample Batié	**207Pb/235U**	**1σ %**	**206Pb/238U**	**1σ %**	**206Pb/238U**	**1σ %**	**207Pb/235U**	**1σ %**	**207Pb/206Pb**	**Rho**
Batié Ga	0.7887	1.8	0.0956	1.59	590	18	591	16	532	0.74
Batié A	0.7743	1.9	0.0956	1.88	589	21	582	17	568	0.67
Batié Ga"	0.772	1.7	0.0957	1.5	589	17	581	15	522	0.74
Batié Gb'	0.7927	2	0.0963	1.25	593	14	594	18	542	0.52
Batié Gb	0.7926	2.5	0.0988	1.42	611	16	594	22	562	0.71
Batié Ga'	0.8352	2	0.0992	1.61	612	19	623	20	660	0.71
Batié F	0.8868	1.7	0.1009	1.72	620	20	645	16	656	0.72
Batié D	0.8629	1.8	0.1028	1.76	631	21	632	17	606	0.7
Batié A	0.8611	2	0.1035	1.73	635	21	631	19	620	0.68
Batié Gc'	0.8812	3.1	0.1048	1.13	645	14	642	30	620	0.82
Batié C	0.8829	1.9	0.1059	1.81	649	22	643	18	598	0.84
Batié Gc	0.9585	1.7	0.1062	1.14	653	14	687	17	740	0.62

229-310 in fine-grained granite) in the investigated granitoids indicating high temperature (741 to 838°C) for their formation. Harris *et al*. (1993) [60] found that high Rb/Sr (4-10) suggests granite formation by dehydration melting, whereas Rb/Sr ratios <4 suggest vapor-present melting. Accordingly, it appears that most of the investigated granitoids (Rb/Sr <4; Table **5**) formed by vapor-present melting. Lower Rb/Sr ratios <4 suggests the participation of biotite during melt production of the granitoids [61, 62]. The strong positive correlation between Zr *vs* Sr and TiO_2 *vs* Sr in the Bapa-Batié plutonic rocks (Fig. **14**) is best explained by different degrees of partial melting due to increasing temperature [63, 64].

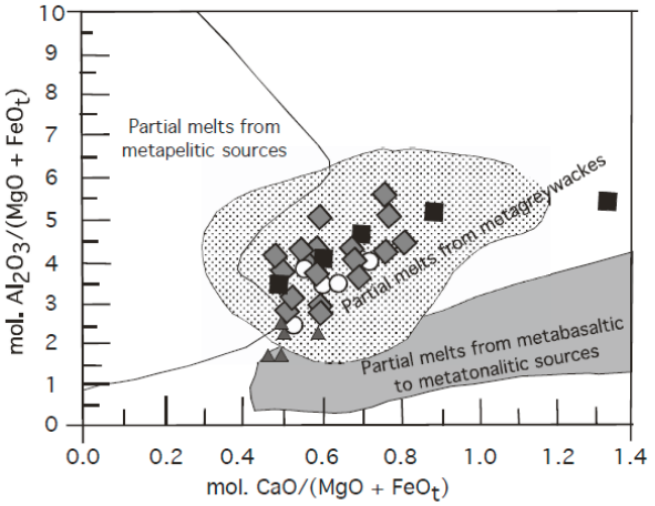

Fig. (13). Molar CaO/ (MgO +FeO_t) *vs* Al_2O_3/ (MgO +FeO_t) for the Bapa-Batié granitoids. Symbols as in Fig. (**4**).

Implications for the Assembly of Western Gondwana

The results of this study and the recent works by Pimentel *et al*. (2001) [65], Piuzana *et al*. (2003) [66], Neves *et al*., 2006 [43] and Ferré *et al*. (2002) [37] on the geodynamic evolution of NE and Central Part of Brazil and Nigeria, respectively, strengthen the previous suggestion [4, 9, 11, 21] that these belts shared a common evolution throughout most of the Proterozoic. Common features include (i) distensive Palaeoproterozoic crust (ca. 2.1Ga), (ii) dominance of metasedimentary sequences with Neoproterozoic deposition ages, (iii) ubiquitous presence of flat-lying structures of Neoproterozoic age (~650-600 Ma), and, (iv) dominance of transpressional/transcurent deformation After 600 Ma. The lack of evidence for closure of wide oceanic domains in all these regions does not support the interpretation of the central and south domains of the PANEFB as a series of amalgamated terranes [18]. Destabilisation of a pre-existing continent that formed at the end of Paleoproterozoic/Eburnean orogeny [67] provides the simplest explanation to the above findings. An ultimate period of plate-wide extension occurred in the mid/late Neoproterozoic. This was immediately followed by convergence and contractional deformation marking the beginning of the Pan-African/Brasiliano orogeny, which essentially occurred in an intracontinental setting.

CONCLUSION

1. Plutonic rocks from the Bapa-Batié area are high-K, calc-alkaline to shoshonitic syntectonic intrusions that were emplaced during a Neoproterozoic event at 600-619Ma in Cameroon, in close spatial association with the Central Cameroon Shear Zone.

2. The elongate form of the plutons, consistent with the regional strike, demonstrates syn-kinematic magma emplacement during the Pan-African orogeny.

3. The data presented in this study are consistent with magmatism that may have involved remelting (biotite dehydration melting) of a composite metagreywacke protolith in the upper crust in the Central domain of the PANEFB.

4. Structural and geochemical characteristics indicate that the Bapa-Batié complex is part of the syn-collisional

Table 8. LA-ICP-MS U-Pb Results for Zircons from Biotite-Amphibole Granite of the Bapa-Batié Area

	Isotopic Ratios				Apparent Ages (Ma)						
Sample CM8	**207Pb/235U**	**1σ %**	**206Pb/238U**	**1σ %**	**206Pb/238U**	**1σ %**	**207Pb/235U**	**1σ %**	**207Pb/206Pb**	**1σ %**	**Rho**
CM8GJ'	0.7823	2.2	0.0936	1.41	577	16	587	19	610	92	0.35
CM8 c"	0.8776	3.5	0.0938	1.81	578	20	640	33	764	98	0.8
CM8Gi"	0.8005	2	0.0945	1.3	582	14	597	18	656	58	0.74
CM8Gf'	0.7826	1.5	0.0946	1.41	582	16	587	13	560	52	0.65
CM8Gh'	0.7721	2.5	0.0948	1.58	584	18	581	22	560	78	0.72
CM8 j'	0.7788	2.9	0.0948	1.35	584	15	585	26	610	84	0.8
CM8Gi'	0.7738	2.2	0.095	1.48	585	17	582	19	556	78	0.59
CM8Gc	0.8338	2.1	0.095	1.51	585	17	616	20	692	68	0.65
CM8Gj"	0.7914	1.9	0.0952	1.44	586	16	592	17	570	64	0.66
CM8 i	0.7699	3.1	0.0953	1.7	587	19	580	28	526	118	0.51
CM8Ge"	0.7862	1.7	0.0955	1.52	588	17	589	15	564	54	0.71
CM8 a	0.7806	2.3	0.0956	1.64	588	18	586	20	572	82	0.56
CM8 f	0.8448	2.8	0.0958	1.42	590	16	622	26	624	92	0.65
CM8Gi	0.7992	1.6	0.0959	1.84	590	21	596	15	580	62	0.68
CM8 i	0.8126	2.1	0.0959	1.64	590	19	604	19	570	74	0.6
CM8Ge	0.8043	2	0.096	1.46	591	16	599	18	564	62	0.68
CM8Gh	0.8032	1.5	0.0961	1.38	592	16	599	14	586	48	0.68
CM8 f'	0.8083	2.3	0.0963	1.35	593	15	602	21	588	68	0.76
CM8 e'	0.8143	2.8	0.0965	1.55	594	18	605	25	604	100	0.54
CM8 e	0.8425	2.6	0.0968	1.55	596	18	621	24	642	92	0.57
CM8Gg'	0.8035	2	0.0969	1.37	596	16	599	18	594	68	0.61
CM8 b'	0.8425	3.1	0.097	1.81	597	21	621	29	628	92	0.74
CM8Gg	0.7802	2.1	0.0971	1.58	598	18	586	19	476	62	0.74
CM8Gf	0.8071	1.7	0.0972	1.36	598	16	601	15	568	56	0.66
CM8 h	0.8373	1.7	0.0972	1.38	598	16	618	16	608	74	0.39
CM8 h'	0.8201	1.9	0.0975	1.51	600	17	608	17	616	68	0.58
CM8 j	0.7898	2.5	0.0975	1.41	600	16	591	23	534	88	0.61
CM8 a'	0.841	3.8	0.0976	1.7	600	19	620	35	656	106	0.87
CM8Gb"	0.8578	1.6	0.0977	1.53	601	18	629	15	738	66	0.51
CM8 c'	0.7956	3.3	0.0978	1.83	601	21	594	30	514	114	0.63
CM8 c"'	0.8566	2.5	0.0979	1.58	602	18	628	23	594	96	0.48
CM8Ge'	0.7978	2.1	0.0982	1.33	604	15	596	19	544	72	0.63
CM8 d'	0.8397	3.7	0.0983	1.75	605	20	619	34	608	102	0.84
CM8Gg"	0.822	1.4	0.0985	1.31	606	15	609	13	600	48	0.65
CM8Gb'	0.8048	2	0.0985	1.42	605	16	600	18	612	72	0.56
CM8Gd	0.8072	2.3	0.0989	1.47	608	17	601	20	576	76	0.64
CM8 c	0.7503	2.6	0.0989	1.68	608	20	568	22	402	86	0.68
CM8 d	0.8156	2.4	0.0991	1.54	609	18	606	22	518	84	0.62
CM8 g'	0.8308	3.9	0.0992	1.78	610	21	614	36	578	128	0.7
CM8 b	0.7677	3.1	0.1002	1.83	615	22	578	27	378	114	0.58
CM8 a"	0.8402	3	0.1003	1.46	616	17	619	28	594	106	0.59
CM8Gb	0.805	2.4	0.1004	1.4	617	17	600	22	528	80	0.67
CM8 b	0.8178	3.2	0.1012	1.75	621	21	607	29	502	114	0.59
CM8Gd'	0.8252	1.9	0.1013	1.32	622	16	611	18	556	64	0.67
CM8 g	0.778	3	0.1017	1.6	624	19	584	27	450	112	0.57
CM8Gc'	0.8848	2.2	0.1027	1.44	630	17	644	21	716	92	0.39
CM8 j"	0.8237	2	0.1043	1.49	640	18	610	18	500	70	0.61

magmatism emplaced in the course of Pan-African deformation during late-orogenic uplift and extension. The plutonic rocks of the Bapa-Batié area are very similar to other Neoproterozoic high-K calc-alkaline syntectonic plutons from western and central east Cameroon in modal, major and trace element characteristics. Most of these features are found in the Borborema Province of NE Brazil [43] and in the Nigeria Province [37], indicating a shared evolution during most of the Proterozoic. Roughly similar syntectonic plutonism in relation with lithospheric-scale shear zone is also observed in NE Brazil, especially close to the Pernambuco Shear Zone.

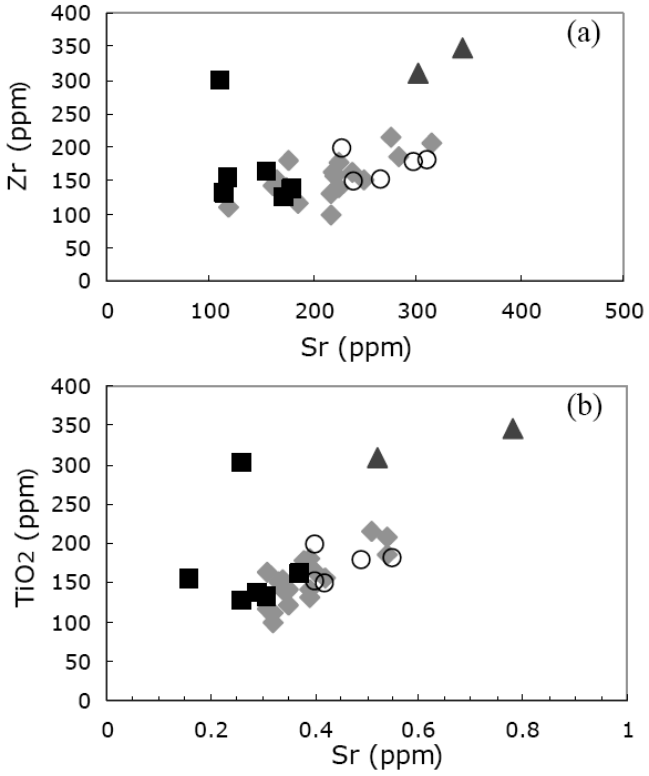

Fig. (14). Zr *vs* Sr and TiO_2 *vs* Sr variation diagrams for the Bapa-Batié granitoids. Symbols as in Fig. (**4**).

ACKNOWLEDGEMENTS

Thanks are due to Professor L. Baumgartner, Institute of Mineralogy and Geochemistry, University of Lausanne, Switzerland for providing many facilities.

REFERENCES

[1] B. Barbarin, "A review of the relationships between granitoids types, their origins and their geodynamic environments", *Lithos*, vol. 46, pp. 605-626, 1999.

[2] D.H.W. Hutton, and T.J. Dempster, P.E. Brown, S.D. Becker, "A new mechanism of emplacement: intrusion in active extensional shear zones", *Nature*, vol. 343, pp. 452-455,1990.

[3] J.P. Nzenti, "*L'Adamaoua panafricain (région de Banyo) : une zone clé pour un modèle de la chaîne panafricaine nord-équatoriale au Cameroun"*, Thèse Doct. D'Etat, Univ Cheikh Anta Diop -Univ Nancy I, France, 1998.

[4] J.P. Nzenti, P. Barbey, J.M. Bertrand, and J. Macaudière, "La chaîne panafricaine au Cameroun : cherchons suture et modèle!" In: *S. G. F.* Ed. *15ème Réunion des Sciences de la Terre*, Nancy, France, pp. 99, 1994.

[5] J.P. Nzenti, B. Kapajika, G. Wörner, and R.T. Lubala "Synkinematic emplacement of granitoids in a Pan-African shear zone in Central Cameroon", *J. Afr. Earth Sci.*, vol. 45, pp. 74-86, 2006.

[6] J.P. Nzenti, E.L. Tankonjiosseu, and A. Nzina Nchare, "The metamorphic evolution of the Paleoproterozoic high grade Banyo gneisses (Adamawa, Cameroon, Central Africa)", *J. Camer. Acad. Sci.*, vol. 7, pp. 95-109, 2007.

[7] T. Ngnotué, J.P. Nzenti, P. Barbey, and F.M. Tchoua "The Ntui-Bétamba high-grade gneisses: a northward extension of the Pan-African Yaoundé gneisses in Cameroon", *J. Afr. Earth Sci.*, vol. 31, pp. 369-381, 2000.

[8] V. Ngako, P. Afrfaton, J.M. Nnange, T. Njanko, "Pan-African tectonic evolution in central and southern cameroon : transpression and transtension during sinistral shear movements", *J. Afr. Earth Sci.*, vol. 36, pp. 207-214, 2003.

[9] E.L. Tankonjiosseu, J.P. Nzenti, T. Njanko, B. Kapajika, and A. Nédelec, "New U-Pb zircon ages from Tonga (Cameroon): coexisting Eburnean-Transamazonian (2.1 Ga) and Pan-African (0.6 Ga) imprints", *C. R. Géosci.*, vol. 337, pp. 551-562, 2005.

[10] S.F. Toteu, J. Penaye, Y.H. Djomani Poudjom, "Geodynamic evolution of the Pan-African belt in central Africa with special reference to Cameroon," *Can. J. Earth Sci.*, vol. 41, pp. 73-85, 2004.

[11] J.P. Nzenti, P. Barbey, J. Macaudière, and D. Soba, "Origin and evolution of late Precambrian high-grade Yaoundé gneisses (Cameroon)", *Precam. Res.*, vol. 38, pp. 91-109, 1988.

[12] J. Penaye, S.F. Toteu, W.R. Van Schmus, J.P. Nzenti, "U-Pb and Sm-Nd preliminary geochronologic data on the Yaoundé series, Cameroon: re-interpretation of the granulitic rocks as the suture of a collision in the centrafrican belt", *C. R. Acad. Sci. Paris*, vol. 317, pp. 789-794, 1993.

[13] J.P. Nzenti, "Neoproterozoic alkaline meta-igneous rocks from the Pan-African North Equatorial fold belt (Yaoundé, Cameroon): biotitites and magnetite rich pyroxenites", *J. Afr. Earth Sci.*, vol. 26, pp. 37-47, 1998.

[14] J.P. Nzenti, P. Barbey, P. Jegouzo, and C. Moreau, "Un nouvel exemple de ceinture granulitique dans une chaîne Protérozoïque de collision: les migmatites de Yaoundé au Cameroun", *C. R. Acad. Sci.*, vol. 299/17, pp. 1197-1199, 1984.

[15] C. Castaing, J.L. Feybesse, D. Thiéblemont, C. Triboulet, and P. Chèvremont, "Palaeogeographical reconstructions of the Pan-African/Brasiliano orogen: closure of an oceanic domain or intracontinental convergence between major blocks?" *Precam. Res.*, vol. 69, pp. 327-344, 1994.

[16] B.B Brito Neves, W.R. Van Schmus, A. Fetter, "North-western Africa-North eastern Brazil : major tectonic links and correlation problems", *J. Afr. Earth Sci.*, vol. 34, pp. 275-278, 2002.

[17] U.G. Cordani, M.S. D´Agrella-Filho, B.B. Brito-Neves, R.I.F. Trindale, "Tearing up Rodinia: the Neoproterozoic palaeogeography of South American cratonic fragments", *Terra Nova*, vol. 15, pp. 350-359, 2003.

[18] E. Njonfang, V. Ngako, C. Moreau, P. Aғfaton, H. Diot, "Restraining bands in high temperature shear zones: The "Central Cameroon Shear Zone", Central Africa", *J. Afr Earth Sci.*, vol. 52, pp. 9-20, 2008.

[19] T.C. Nguiessi, J.P. Nzenti, E.N. Nsifa, P. Tempier, and F.M. Tchoua, "Les granitoïdes calco-alcalins, syncisaillement de Bandja dans la chaîne pana fricaine nord-équatoriale au Cameroun", *C. R. Acad. Sci.*, vol. 325, pp. 95-101, 1997.

[20] G. Tagne-Kamga, E. Mercier, M. Rossy, and N.E. Nsifa. Synkinematic emplacement of the Pan-African Ngondo igneous complex (west Cameroon, central Africa)," *J. Afr. Earth Sci.*, vol. 28, pp. 675-691, 1999.

[21] C. Nzolang, H. Kagami, J.P. Nzenti, and F. Holtz, "Geochemistry and preliminary Sr-Nd isotopic data on the Neoproterozoic granitoids from the Bantoum area, west Cameroon: evidence for a derivation from a Paleoproterozoic Archean crust", *Polar Geosci.*, vol.16, pp. 196-226, 2003.

[22] M. L. Djouka-Fonkwé, B. Schulz, U. Schüssler, J-P. Tchouankoué, and C. Nzolang, "Geochemistry of the Bafroussam Pan-African I- and S- type granitoids in western Cameroon", *J. Afr. Earth Sci.*, vol. 50, vol., pp. 148-167, 2008.

[23] A. Ganwa, W. Frisch, W. Siebel, S.K. Cosmas, O.J. Mvondo, M. Satir, N.J. Tchakounté, "Zircon ^{207}Pb-^{206}Pb evaporation ages of Pan-African metasedimentary rocks in the Kombé-II area (Bafria Group, Cameroon): constraints on protolith age and provenance", *J. Afr. Earth Sci.*, vol. 51, pp. 77-88, 2008.

[24] D. Tchaptchet Tchato, B. Schulz and J.P. Nzenti, "Electron microprobe (EMP) monazite dating and P-T data of the Neoproterozoic metamorphic and mylonitic events in the Kekem area, Cameroon North Equatorial Fold belt", *N. Jb. Miner. Abh*., vol.186, Issue1, pp. 95-109, 2009.

[25] S.F Toteu, A. Michard, J. M. Bertrand, and G. Rocci, "U/Pb of Precambrian rocks from northern Cameroon, orogenic evolution and chronology of the Panafrican belt of central Africa", *Precamb. Res.*, vol. 37, pp.71-87, 1987.

[26] G. Njiekak, W. Dörr, J-P. Tchouankoué, and G. Zulauf, "U-Pb zircon and microfabric data of (meta) granitoids of western Cameroon: constraints on the timing of pluton emplacement and deformation in the Pan-African belt of Central Africa", *Lithos*, vol. 102, pp. 460-477, 2008.

[27] C. Chebeu, "*Igneous emplacement in a transpressive shear zone: Bapa-Batié granitoids (West Cameroon)*", MSc thesis, Univ Yaoundé I, p. 52, 2003.

[28] B. Kankeu, "*Anisotropie de la susceptibilité magnétique (ASM) et fabriques des roches Néoprotérozoiques des régions de Garga-Sarali et Bétaré-Oya à l'Est Cameroon: implications géodynamiques pour l'évolution de la chaîne panafricaine d'Afrique Centrale*", Ph.D. thesis. Université de Yaoundé I, p. 232, 2008.

[29] B. Kankeu, O.R. Greiling, and J.P. Nzenti, "Pan-African strike-slip tectonics in eastern Cameroon. Magnetic fabrics (AMS) and structure in the Lom basin and its gneissic basement (Bétaré Oya)", *Precambr. Res.*, vol. 17, no. 3-4, pp. 258-272, 2009.

[30] G. Witt-Eickschen, H.A. Seck, K. Mezger, S.M. Eggins, and R. Altheer, "Lithospheric mantle evolution beneath the Eifel (Germany): constraints from Sr-Nd-Pb isotopes and trace element abundances in spinel peridotite and pyroxenites xenoliths", *J. Petrol.*, vol. 44, pp. 1077-1095, 2003.

[31] K. R. Ludwig, *User's Manual for Isoplot/Ex v. 3.00. A Geochronological Toolkit for Microsoft Excel*, BGC Special Publication 4, Berkeley, p. 71, 2003.

[32] F. Debon, and M. Lemmet, "Evolution of Mg/Fe ratios in late Variscan plutonic rocks from the external crystalline massifs of the Alps (France, Italy, Switzerland)", *J. Petrol.*, vol. 40, pp. 1151-1185, 1999.

[33] B.R. Frost, C.G. Barnes, W.J. Collins, R.J. Arculus, D.J. Ellis, and C.D. Frost, "A geochemical classification for granitic rocks", *J. Petrol.*, vol. 42, pp. 2033-2048, 2001.

[34] J.M. Bertrand, C. Dupuy, J. Dostal, and I. Davidson, "Geochemistry and geotectonic interpretation of granitoids from Central Iforas (Mali, West Africa)", *Precamb. Res*., vol. 26, pp. 265-283, 1984.

[35] R. Ayuso, and J.G. Arth, "The Northeast Kingdom batholith, Vermon: magmatic evolution and geochemical constraints on the origin of Acadian granitic rocks", *Contrib. Miner. Petrol.*, vol. 111, pp. 1-23, 1992.

[36] S.S. Dada, L. Briqueu, U. Harms, J.R. Lancelot, and G. Matheis, "Charnockitic and monzonitic Pan-African series from north-central Nigeria: trace-element and Nd, Sr, Pb isotope constraints on their petrogenesis", *Chem. Geol*., vol. 124, pp. 233-252, 1995.

[37] E. Ferré, G. Gleizes, and R. Caby, "Obliquely convergent tectonics and granite emplacement in the Trans-Saharan belt of eastern Nigeria: a synthesis", *Precambr. Res.*, vol. 114, pp. 199-219, 2002.

[38] V.O. Olarewaju, and M.A. Rahaman, "Petrology and geochemistry of older granites from some parts of northern Nigeria", *Niger. J. Min. Geol.*, vol. 18, pp. 16-28, 1982.

[39] V.P. Ferreira, A.N. Sial, M.M. Pimentel, and C.A.V. Moura, "Intermediate to acidic magmatism and crustal evolution in the Transversal Zone, north-eastern Brazil", In: V. Mantesso-Neto, A. Bartorelli, C. Carneiro, B.B. Brito-Neves, Eds., *Geologia do continente Sul-Americano: evolução da obra de Fernando Flàvio Marques de Almeida*. Beca, São Paulo, Brazil, 2004, pp. 189-201.

[40] G. Mariano, P.B. Correia, S.P. Neves, and A.F.D. Silva Filho, "The high-K calc-alkaline Alagoinhas pluton: anisotropy of magnetic susceptibility, geochemistry, emplacement setting, and implications for the evolution of Borborema Province, NE Brazil", *Int. Geol. Rev.*, vol. 51, pp. 502-519, 2009.

[41] S. P. Neves, and G. Mariano, "High-K calc-alkalic plutons in NE Brazil: origin of the biotite diorite/quartz monzonite to granite association and implications for the evolution of the Borborema Province", *Inter. Geol. Rev*., vol. 39, pp. 621-638, 1997.

[42] S.P. Neves, A. Vauchez, and C.J. Archanjo. "Shear zone-controlled magma emplacement or magma-assisted nucleation of shear zones"? Insights from northeast Brazil. *Tectonophysics*, vol. 262, pp. 349-364, 1996.

[43] S. P. Neves, O. Bruguier, A. Vauchez, D. Bosch, J.M.R Silva, and G. Mariano, "Timing of crust formation, deposition of supracrustal sequences, and Transamazonian and Brasiliano metamorphism in the East Pernambuco belt (Borborema Province, NE Brazil): Implications for western Gondwana assembly", *Precambr. Res.*, vol. 149, pp. 197-216, 2006.

[44] J.A. Pearce, "Trace element characteristics of lavas from destructive plate boundaries", in R.S. Thorpe, Ed., *Andesites*. London, John Wiley, 1982, pp. 525-548.

[45] T.M. Harrison, and B. Watson, "Kinetics of zircon dissolution and zirconium diffusion in granitic melts of variable water content". *Contrib. Miner. Petrol.*, vol. 84, pp. 66-72, 1983.

[46] E.B. Watson, and T.M. Harrison, "Zircon saturation revisited: temperature and composition effects in a variety of crustal magma types", *Earth Planetary Sci Lett*, vol. 64, pp. 295-304, 1983.

[47] B.W. Chappell, and A.J.R.White, "Two contrasting granite types", *Pacific Geol*., vol. 8, pp. 173-174, 1974.

[48] B.W. Chappell, and A.J.R.White, "I- and S-type granites in the Lachlan Fold Belt", *Trans. Roy. Soc. Edinburgh*, vol. 83, pp. 1-12, 1992.

[49] F.F. Altherr, A. Holl, E. Hegner, C. Langer, and H. Kreuzer, "High-potassium, calc-alkaline I-type plutonism in the European variscides: northern Vosges (France) and northern Schwarzwald (Germany)", *Lithos*, vol. 50, pp 51-73, 2000.

[50] D.J. De Paolo, "A neodymium and strontium isotopic study of the Mesozoic calc-alkaline granitic batholiths of the Sierra Nevada and Peninsular Ranges, California", *J. Geophys. Res*, vol. 86 (B11), pp. 10470-10488, 1981.

[51] M.P. Roberts, and J.D. Clemens, "Origin of high-potassium, calc-alkaline, I-type granitoids", *Geology*, vol. 21, pp. 825-828, 1993.

[52] J.P. Liégeois, R. Black, J. Navez, and L. Latouche "Early and late pan African orogenies in the Aïr assembly of terranes (Tuareg Shield, Niger)", *Precamb. Res*., vol. 67, pp. 59-88, 1994.

[53] M.P. Roberts, C. Pin, J.D. Clemens, and J.L. Paquette, "Petrogenesis of mAfric to felsic plutonic rock associations: the calc-alkaline Quérigut complex, French pyrénées", *J. Petrol*., vol. 41, issue 6, pp. 808-844, 2000.

[54] J. M. Montel, and D. Vielzeuf, "Partial melting of metagreywackes. Part 2. Compositions of mineral and melts", *Cont. Mineral. Petrol*., vol. 128, pp. 176-196, 1997.

[55] A.E Patiño Douce, and J. S. Beard, "Effects of P, f(O_2) and Mg/Fe ratio on dehydratation melting of model metagreywackes", *J. Petrol*., vol. 37, pp. 999-1034, 1996.

[56] A.F.D. Silva Filho, I.P. Guimaraes, M.F.L.D. Brito, and M.M. Pimental, "Geochemical signatures of main Neoproterozoic Late-tectonic granitoids from the Proterozoic Sergipano fold belt, Brazil: significance for the Brasiliano orogeny", *Intern. Geol. Rev*., vol. 39, pp 639-659, 1997.

[57] S. P. Neves, and G. Mariano, "The lithospheric mantle as a source of magmas during orogenic processes: insights from high-K diorites in the Borborema Province and implications for continental dynamics", *J. Virt. Expl.*, vol. 17, pp. 1-14, 2004.

[58] E. Ferré, R. Caby, J.J. Peucat, R. Capdevila, and P. Monié, "Pan-African, post-collisional, ferro-potassic granite and quartz-monzonite plutons of eastern Nigeria", *Lithos*, vol. 45, pp. 255-279, 1998.

[59] K.T. Winther, and R.C. Newton, "Experimental melting of hydrous low-K tholeiites: evidence of the origin of Archean cratons", *Geol. Soc. Denmark Bull*., vol. 39, pp. 213-228, 1991.

[60] N.B.W. Harris, S. Inger, and J. Massey, "The role of fluids in the formation of High Himalayan leucogranites". In: Treloar PJ, Searle MP (eds) Himalayan tectonics. *Spec. Publ. Geol. Soc*. Lond., vol. 74, pp. 391-400, 1993.

[61] S. Inger, and N.B.W. Harris, "Geochemical constraints on leucogranites magmatism in the Lantang valley, Nepal Himalaya", *J. Petrol*,. 34, 345-368, 1993.

[62] T.M. Harrisson, M. Grove, K.D. McKeegan, C.D. Coath, O.M. Lovera, and P. Le Fort, "Origin and episodic emplacement of the Manaslu intrusive complex, central Himalaya", *J. Petrol*., vol. 40, pp. 3-19, 1999.

[63] D. Visona, and B. Lombardo, "Two micas and tourmaline leucogranites from the Everest-Macalu region (Nepal-Tibet).

Himalayan leucogranites genesis by isobaric heating?" *Lithos*, vol. 62, pp. 125-150, 2002.

[64] A. M. Moghazi, M. A. Hassanen, F. H. Mohamed, and S. Ali, "Late Neoproterozoic strongly peraluminous leucogranites, South Eastern Desert, Egypt. Petrogenesis and geodynamic significance", *Mineral. Petrol*., vol. 81, pp. 19-41, 2004.

[65] M. M. Pimentel, M. A. Dardenne, R. A. Fuck, M. G. Viana, S.L. Junges, D. P. Fischel, H.J. Seer, and E. L. Dantas, "Nd isotopes and the provenance of detrital sediments of the Neoproterozoic Brasilia Belt, central Brazil", *J. South Am. Earth Sci.*, vol. 14, pp. 571-585, 2001.

[66] D. Piuzana, M. M. Pimentel, R. A. Fuck, and R. Armstrong, "Neoproterozoic granulite facies metamorphism and coeval granitic magmatism in the Brasília Belt, central Brazil: regional implications of new SHRIMP U-Pb and Sm-Nd data", *Precambr. Res.* Vol. 125, pp. 245-273, 2003.

[67] J.J.W. Rogers, "A history of continents in the past three billion years", *J. Geol*., vol. 104, pp. 91-107, 1996.

[68] R. Caby, A.N. Sial, M. Arthaud, and A. Vauchez, "Crustal evolution and the Brasiliano orogeny in northeast Brazil.- in : R. D. Dallmeyer and J. P. Lécorché, Eds. The west African orogens and circum-Atlantic correlatives", *Springer-Verlag*, Berlin, pp. 373-397, 1991.

[69] D. Soba "*La série de Lom: Etude Géologique et Géochronologique d'un bassin volcano-sédimentaire de la Chaîne PanAfricaine à l'Est du Cameroun*", Thèse Doctorat D'Etat, Université de Paris VI, 198p, 1989.

[70] A. L., Streckeisen, "Classification of the common igneous rocks by means of their chemical composition: a provisional attempt". Neues Jahrbuch fur Mineralogie, Monatshefte, vol. H. 1, pp. 1-15, 1976.

[71] R.W. Le Maitre, P. Bateman, A. Dudek, J. Keller, J. Lameyre, M.J. Le As, P.A. Sabine, R. Schmid, H. Sorensen, A. Streckeisen, A.R. Ooley, and B. Zanettin, "A classification of igneous rocks and glossary of terms", *Blackwell, Oxford,* 1989.

[72] P.C. Rickwood, "Boundary lines within petrologic diagrams which use oxides of major and minor elements", *Lithos*, vol. 22, pp. 247-263, 1989.

[73] N.M. Evensen, M.J. Hamilton, and R.J. O´Nions, "Rare earth abundances in chondritic meteorites", *Geochem Cosmochim Acta*, vol. 42, pp. 1199-1212, 1978.

Received: March 10, 2010 Revised: May 13, 2010 Accepted: August 17, 2010